International Journal of Solids and Structures 49 (2012) 492–513

Contents lists available at SciVerse ScienceDirect

International Journal of Solids and Structures

journal homepage: www.elsevier.com/locate/ijsolstr

A continuum damage mechanics framework for modeling micro-damage healing

Masoud K. Darabi, Rashid K. Abu Al-Rub *, Dallas N. Little

Zachry Department of Civil Engineering, Texas A&M University, College Station, TX 77843, USA

ARTICLE INFO

Article history:
Received 19 February 2011
Received in revised form 29 August 2011
Available online 25 October 2011

Keywords:
Micro-damage healing
Continuum damage mechanics
Rest time
Healing natural configuration
Thermodynamic-based constitutive modeling

ABSTRACT

A novel continuum damage mechanics-based framework is proposed to model the micro-damage healing phenomenon in the materials that tend to self-heal. This framework extends the well-known Kachanov's (1958) effective configuration and the concept of the effective stress space to self-healing materials by introducing the healing natural configuration in order to incorporate the micro-damage healing effects. Analytical relations are derived to relate strain tensors and tangent stiffness moduli in the nominal and healing configurations for each postulated transformation hypothesis (i.e. strain, elastic strain energy, and power equivalence hypotheses). The ability of the proposed model to explain micro-damage healing is demonstrated by presenting several examples. Also, a general thermodynamic framework for constitutive modeling of damage and micro-damage healing mechanisms is presented.

1. Introduction

Kachanov (1958) pioneered the concept of the effective (undamaged) configuration and introduced the basis for the continuum damage mechanics theories. Followed by his pioneering work, many researchers have used the effective configuration concept to model the irreversible damage processes in engineering materials (e.g. Kachanov, 1958; Rabotnov, 1969a; Lemaître and Chaboche, 1990; Voyiadjis and Kattan, 1999). However, experimental observations in the last decade have clearly shown that various classes of engineering materials have the potential to heal and retrieve part of their strength and stiffness under specific conditions (Miao et al., 1995; Kessler and White, 2001; Brown et al., 2002; Reinhardt and Jooss, 2003; Guo and Guo, 2006; Kessler, 2007; Bhasin et al., 2008). The intrinsic healing capability of biomaterials and biological systems is a well-known and well-established fact (e.g. Yasko et al., 1992; Rodeo et al., 1993; Arrington et al., 1996; Strauer et al., 2002; Werner and Grose, 2003). Moreover, several procedures for synthesizing self-healing polymers are recently developed inspired by these unique features of biological systems and materials (e.g. White et al., 2001; Brown et al., 2005; Bond et al., 2007; Rong et al., 2007; White et al., 2008; Yin et al., 2008; Yuan et al., 2008). Another category of the engineering materials that tend to heal is the composite materials whose matrix is intrinsically tend to heal at elevated temperatures and during the rest periods (e.g. Little and Bhasin, 2007; Bhasin et al., 2008, 2010). Interestingly, from the continuum point of view, the common feature of the healing phenomenon in all of these materials (e.g. self-healing polymers and biomaterials) is that the induced micro-damages (e.g. microcracks, micro-voids) gradually reduce in size and subsequently cause the material to recover partially or fully its strength and stiffness. Therefore, it seems quite natural to relate the modeling of the healing phenomenon to the size and density of the healed micro-damages.

Several attempts have been made in the literature for constitutive modeling of the micro-damage healing phenomenon in materials. These attempts are mostly phenomenological (e.g. Jacobsen et al., 1996; Ramm and Biscoping, 1998; Adam, 1999; Simpson et al., 2000; Ando et al., 2002; Little and Bhasin, 2007). Few thermodynamic-based micro-damage healing models are available in the literature. Miao et al. (1995) proposed a constitutive model for compaction of crushed rock salts; Alfredsson and Stigh (2004) proposed a fairly general thermodynamic framework for constitutive modeling of elastic, plastic, damage, and healing mechanisms of materials; Barbero et al. (2005) proposed a thermodynamic-based continuum damage-healing constitutive model for self-healing composites; and Voyiadjis et al. (2011) extended the work of Barbero et al. (2005) by incorporating the isotropic hardening due to damage and healing. However, these thermodynamic-based models are formulated for specific micro-damage healing mechanisms. Therefore, they cannot be treated as general frameworks that can be followed systematically to derive different micro-damage healing models. The model proposed by Barbero et al. (2005) is applicable to materials with autonomous micro-damage healing mechanism, where micro-damage healing agents are embedded in the materials and healing can be activated during the loading and during the crack propagation (e.g. White et al.,

* Corresponding author. Tel.: +1 979 862 6603; fax: +1 979 845 6554.
E-mail address: rabualrub@civil.tamu.edu (R.K. Abu Al-Rub).

0020-7683/$ - see front matter © 2011 Elsevier Ltd. All rights reserved.
doi:10.1016/j.ijsolstr.2011.10.017

2001). The models proposed by Miao et al. (1995) and Alfredsson and Stigh (2004) are, on the other hand, applicable to materials for which healing occurs during the rest period and unloading. However, this paper treats the micro-damage healing generally as the reduction of the damaged area and damage density regardless of the specific type of healing. Also, it should be emphasized that the derived micro-damage healing evolution function based on the current framework will be different depending on the healing mechanism and material under study.

Another important issue in formulating a thermodynamic-based micro-damage healing model based on continuum damage mechanics is the postulated transformation hypothesis that relates stresses and strains in the damaged and undamaged (effective) states of the material. Most of the proposed thermodynamic-based damage and healing models are either based on the strain equivalence hypothesis (e.g. Alfredsson and Stigh, 2004) or the elastic energy strain equivalence hypothesis (e.g. Voyiadjis et al., 2011) which are suitable for simple constitutive models such as elastic solids. However, a more realistic transformation hypothesis is required for more complex constitutive models. To generalize the proposed healing framework, this study investigates the effect of postulating different transformation hypotheses on the mechanical response of materials. Moreover, the current thermodynamic framework is formulated based on the power equivalence hypothesis that is more physically sound and can be applied for coupling damage and micro-damage healing models to viscoelasticity and viscoplasticity models as well.

Furthermore, another challenging task is to formulate a general thermodynamic framework that properly estimates the stored and dissipated energy during the damage and micro-damage healing processes. As stated by Ziegler (1977) in his celebrated book on continuum thermodynamics, the proper estimation of the stored and dissipated energies during a process requires the decomposition of the thermodynamic conjugate forces into energetic and dissipative components. The energetic components are responsible for storing energy inside the material and can be identified from a thermodynamic state potential such as the Helmholtz free energy function; whereas, the dissipative components are responsible for dissipating energy and can be identified using another thermodynamic state potential such as the rate of the energy dissipation function. However, none of the previous works decompose the micro-damage healing thermodynamic force into energetic and dissipative components. Obviously, more investigations are required to develop a robust and physically sound thermodynamic-based framework that can be followed systematically to model the micro-damage healing mechanisms in materials that tend to heal.

Therefore, one of the main objectives of this work is to contribute in closing this gap by proposing a general thermodynamic-based framework for constitutive modeling of the micro-damage healing phenomenon that considers physically-based mechanisms associated with the healing process. To this aim, the fundamental basis of the continuum damage mechanics theories based on the effective stress concept (or equivalently based on the effective configuration, Kachanov, 1958; Rabotnov, 1969b) is extended to self-healing materials by introducing a physically-based *natural healing configuration* in order to link the traditional continuum damage mechanics theories to the continuum damage-healing mechanics theories. By following this approach, the proposed framework inherits the simplicity and robustness of the continuum damage mechanics theories (Kachanov, 1958; Rabotnov, 1969b) and also makes it possible to apply the existing numerical techniques for the continuum damage theories to materials that tend to heal without demanding major modifications in the existing numerical algorithms. The proposed framework shows that the thermodynamic forces conjugate to the defined damage and micro-damage healing internal state variables should have both energetic and dissipative components. Furthermore, the proposed general framework derives a *microforce healing balance*, which is shown to be a direct consequence of postulating the principle of virtual power. This newly formulated micro-force balance, along with the decomposition of the healing thermodynamic driving force into energetic and dissipative components, allow one to systematically derive micro-damage healing evolution functions. The proposed framework naturally results in strong couplings between the healing process and temperature evolution. Also, the well-known transformation hypotheses of continuum damage mechanics from the effective (undamaged) to the nominal (damaged) configurations are also considered for the proposed micro-damage healing framework and analytical relations are derived to relate the stiffness moduli in different configurations.

Moreover, the common modeling practice in predicting the damage evolution and growth in the context of continuum damage mechanics is to treat the damage nucleation and growth analogously to time-independent plasticity by introducing a damage surface (analogous to the yield surface) which determines the damage nucleation criterion and a damage evolution function which quantifies the damage density (Kachanov, 1986; Lemaître and Chaboche, 1990; Voyiadjis and Kattan, 1990; Krajcinovic, 1996). This modeling treatment of continuum damage mechanics yields to the fact that damage does not evolve during the unloading where the material point is located in the damage loading surface. Subsequently, the stiffness modulus remains constant during the unloading resulting in a linear response in the stress–strain diagram during the unloading. Fig. 1 shows a schematic representation of the stress–strain response for a complete unloading–loading cycle (e.g. Karsan and Jirsa, 1969). As shown schematically in Fig. 1 and has also been reported in numerous experimental studies on engineering materials, the stress–strain response during the unloading (path "BC" in Fig. 1) is nonlinear (e.g. Sinha et al., 1964; Karsan and Jirsa, 1969; Ortiz, 1985; Bari and Hassan, 2000; Mirmiran et al., 2000; Eggeler et al., 2004; Palermo and Vecchio, 2004; Sima et al., 2008).

In this work, the nonlinear response of the stress–strain diagram during the unloading is related to extra damage growth during the unloading. It should be noted that Ortiz (1985) was the first to model the nonlinear response of the stress–strain diagram during the unloading by considering anisotropic damage and crack closure. The damage anisotropy is not included here; instead, the damage function is allowed to evolve with a slower rate during the unloading to model this distinct behavior. Moreover, the arguments in the subsequent sections show that the underlying

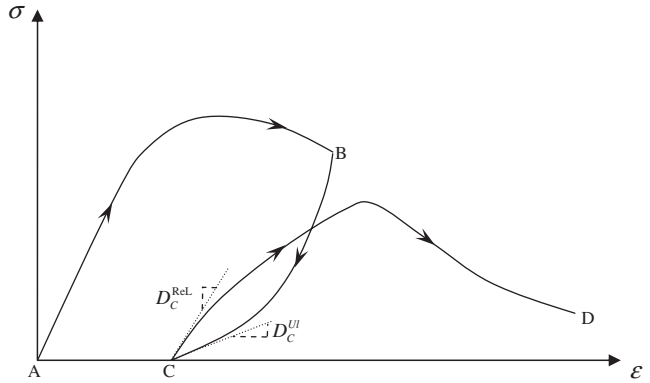

Fig. 1. Schematic representation of the stress–strain response for a loading (path "AB"), unloading (Path "BC"), and reloading (path "CD") cycle. The stress–strain response during the unloading is nonlinear and also the tangent stiffness at the end of the unloading (i.e. D_C^{UI}) is less than the tangent stiffness modulus at the beginning of the reloading (i.e. D_C^{ReL}).

assumptions of this work are physically in line with the fundamental assumptions of Ortiz (1985).

The experimental observations on cyclic loading of several materials show a jump in the tangent stiffness modulus at the unloading–loading points (point "C" in Fig. 1) (Sinha et al., 1964; Karsan and Jirsa, 1969; Ortiz, 1985; Hassan et al., 1992; Eggeler et al., 2004; Sima et al., 2008). In other words, as shown schematically in Fig. 1, the material recovers part of its stiffness at unloading–loading point such that the tangent stiffness at the beginning of the subsequent loading cycle (D_C^{ReL} in Fig. 1) is greater than the tangent stiffness modulus at the end of the unloading (D_C^{UL} in Fig. 1). This jump in the tangent stiffness at the unloading–loading point becomes more significant if rest periods (or unloading times) are introduced between the loading cycles. The current study shows that this distinct behavior could be related to micro-damage healing at low strain levels. In other words, at the end of the unloading, the strain levels becomes close to zero such that the faces of the induced micro-damages wet each other and retrieve part of their bond strength. The wetting of the micro-damage surfaces results in partial healing and subsequently partial recovery in the tangent stiffness modulus at unloading–loading point. This phenomenon is usually referred to as *instantaneous healing* (Wool and Oconnor, 1981). More healing will occur (e.g. due to cohesion and inter-molecular diffusion process between the micro-crack faces in polymers, biomaterials, and bituminous materials) if the wetted surfaces of the micro-damages put into rest for a while before the next loading cycle is applied. This phenomenon is usually referred to as the *time-dependent* (*or long-term*) *healing* in the literature (Wool and Oconnor, 1981).

The numerical examples presented in this work clearly demonstrate the capabilities of the proposed micro-damage healing framework in capturing interesting phenomena such as: (a) the stiffness and strength recovery in cyclic loading upon the application of rest periods; (b) the nonlinear response of the stress–strain diagram during unloading; and (c) the jump in the tangent stiffness modulus at the unloading–loading point.

2. Micro-damage healing configuration

In the classical continuum damage mechanics (CDM) framework, a scalar variable, the damage variable, for the case of the isotropic damage or a higher-order tensor, the damage tensor, for the case of the anisotropic damage is typically used to explain the degradation behavior of materials due to micro-damage (micro-cracks and micro-voids) nucleation and growth (see e.g. Voyiadjis and Kattan, 1999 for a comprehensive review of the this subject). For simplicity and without loss of generality, the case of isotropic damage is considered here. In this paper, the *effective* (*undamaged*) *configuration* is generalized to the cases when materials undergo micro-damage healing or partial/full recovery of the damaged stiffness.

Fig. 2(a) shows a cylinder under a uniaxial tensile load T at the current time "t". During the loading–unloading processes, some new micro-cracks and micro-voids nucleate and propagate upon satisfaction of the damage nucleation and growth conditions. On the other hand, for certain materials (e.g. polymers, bituminous materials, and biological materials) some of these micro-cracks may heal during the resting period (or the unloading process). Therefore, one can divide the total cross-sectional area, A, of the cylinder into three parts: (a) the area that has not been damaged (i.e. intact area), $\overline{A}$, which can be considered as the *effective* (undamaged) area in CDM; (b) the area of unhealed cracks and voids, A^{uh}, where damage is considered irreversible; (c) the area of micro-cracks and micro-voids that have been healed during the unloading process or the rest period, A^h. Fig. 2(b) shows the cross-sectional area of the cylinder at time "t" in the *nominal* (*damaged*) *configuration*. One can assume that the area of the completely healed micro-damages have the same properties of the intact material. Hence, once a micro-crack heals completely, it retrieves all of its strength such that its mechanical properties become identical to those of the intact material. Fig. 2(c) shows the *healing configuration*. This fictitious configuration results when unhealed cracks and voids are removed from the damaged configuration. The *effective* (*undamaged*) *configuration* is shown in Fig. 2(d). This fictitious configuration includes the materials that have never been damaged (intact) during the loading–unloading history. This configuration is identical to the so-called effective configuration in CDM when healing does not occur. Therefore, one can write from Fig. 2:

$$A = \overline{A} + A^D = \overline{\overline{A}} + A^{uh} \tag{1}$$

$$A^D = A^{uh} + A^h \tag{2}$$

where A, $\overline{A}$, and $\overline{\overline{A}}$ are the cross-sectional area in the *nominal* (damaged), *effective* (undamaged), and *healing* configurations, respectively; and A^D is the summation of both healed micro-cracks and micro-voids, A^h, and unhealed micro-cracks and micro-voids, A^{uh}.

As it is assumed in CDM, cracks and voids cannot carry load. In fact, load is carried by the area of the intact material and the healed micro-damages. Therefore, one can assume that the applied forces in the nominal and healing configurations are equal, such that:

$$T = \sigma A = \bar{\bar{\sigma}}\overline{\overline{A}} \tag{3}$$

where σ is the nominal (apparent) stress and $\bar{\bar{\sigma}}$ is the stress in the healing configuration (true or net stress). In this paper, the superscripts "–" and "=" designate the effective and healing configurations, respectively. The following definitions are introduced for the damage and healing internal state variables, respectively:

$$\phi = \frac{A^D}{A} \tag{4}$$

$$h = \frac{A^h}{A^D} \tag{5}$$

For the cases when healing is not considered, ϕ is the classical irreversible damage density variable ranging from $0 \leqslant \phi \leqslant 1$, which is interpreted as the micro-damage density such that $\phi = 0$ indicates no damage and $\phi = 1$ indicates complete damage (or fracture). However, when healing is included, ϕ is interpreted as an internal state variable representing the damage history such that A^D is the accumulative damaged area. On the other hand, h is the *healing internal variable* defined as the ratio of the cumulative area of healed micro-damages over the cumulative damaged area. Therefore, h represents the healed fraction of the total accumulative damaged area. The healing variable ranges from $0 \leqslant h \leqslant 1$; $h = 0$ for no healing and $h = 1$ when all micro-cracks and micro-voids are healed. Alfredsson and Stigh (2004) considered a single damage variable to capture the effect of both damage and micro-damage healing on mechanical response of elastic-plastic materials. The inherent assumption in their work is that the damage and micro-damage healing processes are similar. The approach presented here is more general since it introduces separate internal state variables for the damage and micro-damage healing effects. This would be beneficial for the cases where the driving force for the damage and micro-damage healing mechanisms are different.

Substituting Eqs. (1), (2), (4), and (5) into Eq. (3) yields:

$$\bar{\bar{\sigma}} = \frac{\sigma}{1 - \phi_{eff}} \tag{6}$$

where ϕ_{eff} is the effective damage density ranging from $0 \leqslant \phi_{eff} \leqslant 1$, such that:

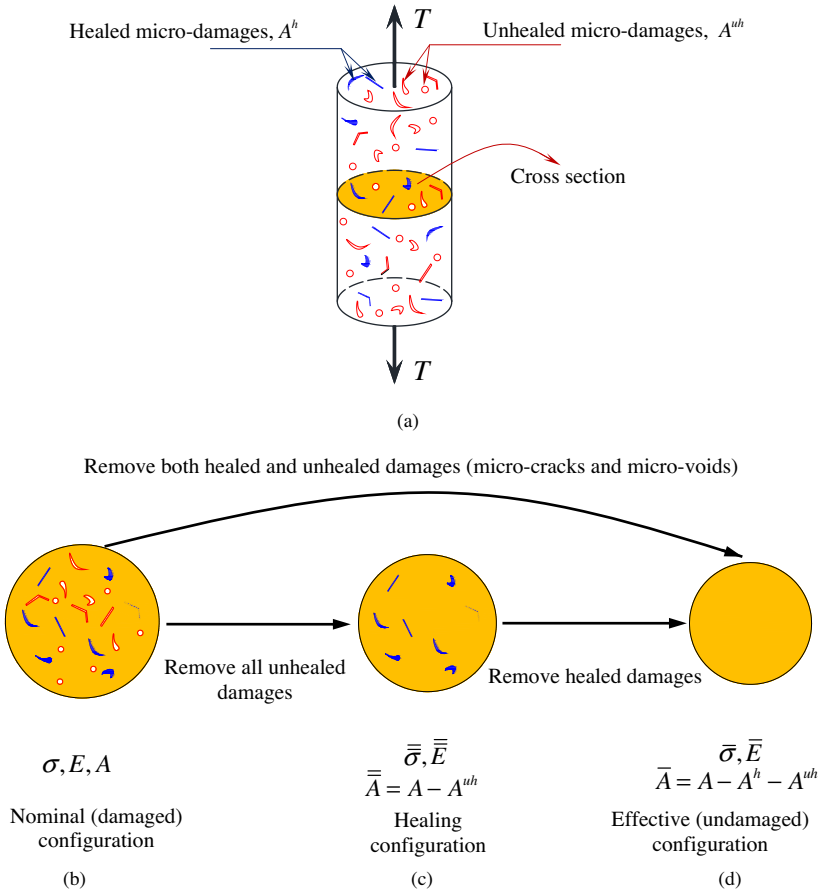

Fig. 2. Schematic representation of: (a) the damaged partially healed cylinder in tension; (b) the nominal configuration; (c) the healing configuration; and (d) the effective configuration. The nominal configuration includes the intact material, unhealed damages, and healed micro-damages; the healing configuration includes the intact material and the healed micro-damages; and the effective configuration only includes the intact material.

$$\phi_{eff} = \phi(1-h) \tag{7}$$

such that $\phi_{eff} = 0$ indicates that either the material has not been damaged yet or all induced damages have already been healed; whereas, $\phi_{eff} = 1$ indicates complete damage (or fracture). It should be noted that the effective damage density variable is no longer irreversible and can decrease upon micro-damage healing.

It is noteworthy that the healing variable in Eq. (7) has a similar effect to the stiffness-recovery parameter introduced in the work of Lee and Fenves (1998) for modeling the stiffness recovery in concrete materials during the transition from tension to compression loading. However, the physics behind the stiffness-recovery parameter by Lee and Fenves (1998) is different than the current proposed micro-damage healing variable h. Lee and Fenves (1998) interpreted the area of healed micro-cracks in Eq. (5), A^h, as the area of closed micro-cracks (not healed) during the loading transition from tension to compression. Therefore, the current proposed healing variable is more general as it can be interpreted as a crack-closure parameter or as a healing parameter, but with a different evolution law, depending on the intended application.

Eqs. (6) and (7) relate the stress in the healing configuration to the nominal stress as a function of the damage and healing internal variables. This expression represents the proper coupling between the damage and healing variables and modifies the classical definition of the effective stress in CDM (i.e. $\bar{\bar{\sigma}} = \bar{\sigma} = \sigma/(1-\phi)$ when healing is not considered (i.e. $h = 0$)).

Eq. (6) can be simply generalized for three-dimensional cases for the case of the isotropic (scalar) damage, such that:

$$\bar{\bar{\boldsymbol{\sigma}}} = \frac{\boldsymbol{\sigma}}{1-\phi_{eff}} = \frac{\boldsymbol{\sigma}}{1-\phi(1-h)} \tag{8}$$

where $\boldsymbol{\sigma}$ is the nominal stress tensor in the damaged configuration and $\bar{\bar{\boldsymbol{\sigma}}}$ is the true stress tensor in the healing configuration.

Moreover, the following relationship between the stress tensors in the healing and effective configurations will be obtained if one assumes that the tensile forces in the effective and healing configurations are the same (i.e. $\bar{\sigma}\bar{A} = \bar{\bar{\sigma}}\bar{\bar{A}}$ in Fig. 2), such that:

$$\bar{\boldsymbol{\sigma}} = \bar{\bar{\boldsymbol{\sigma}}}\left[\frac{1-\phi(1-h)}{1-\phi}\right] \tag{9}$$

Eq. (9) clearly shows that the stress tensors in the healing and effective configurations will be the same only for two cases: (1) damage variable is zero (i.e. $\phi = 0$), where in this case the stress tensors in the effective and healing configurations (i.e. $\bar{\boldsymbol{\sigma}}$ and $\bar{\bar{\boldsymbol{\sigma}}}$) will be the same as the stress tensor in the nominal configuration (i.e. $\boldsymbol{\sigma}$) since damage has not started yet; (2) healing variable is zero (i.e. $h = 0$), where in this case the stress tensors in the effective and healing configurations will be the same since healing is not considered. For other cases, the stress tensor in the fictitious effective configuration will always be greater than the stress tensor in the healing configuration (i.e. $\bar{\boldsymbol{\sigma}} \geqslant \bar{\bar{\boldsymbol{\sigma}}}$). In other words, the effective configuration (Fig. 2(d)) is obtained by removing the healed micro-damage areas from the healing configuration (Fig. 2(c)) such that these healed micro-damages can tolerate load and carry stress in the healing configuration. Therefore, the stress tensor in the effective configurations should be magnified comparing to the stress tensor

in the healing configuration in order to compensate for the stresses carried by the removed healed micro-damages.

In the above, the relations between the stresses in different configurations are derived. In the following sections, the relations among the strain tensors and stiffness moduli in different configurations will be derived.

3. The stiffness moduli in different configurations

As mentioned in Section 2, completely healed micro-cracks and micro-voids recover their total strength and stiffness such that they become identical to the intact material. Hence, one can assume that the stiffness moduli in the effective and healing configurations are the same and equal to the stiffness modulus of the virgin state of the material that does not change during the loading–unloading history, such that:

$$\overline{\boldsymbol{D}} = \overline{\overline{\boldsymbol{D}}} \tag{10}$$

where $\overline{\boldsymbol{D}}$ and $\overline{\overline{\boldsymbol{D}}}$ are the tangent stiffness moduli in the effective and healing configurations, respectively. The tangent stiffness modulus is used in this paper instead of the commonly used secant stiffness modulus in CDM theories. The nominal tangent stiffness modulus is defined as:

$$\boldsymbol{D} = \frac{d\sigma}{d\boldsymbol{\varepsilon}} \tag{11}$$

The secant stiffness modulus is commonly used in CDM to capture the degradation of the stiffness modulus with damage evolution. However, the tangent stiffness modulus could capture the nonlinear response of materials more easily and is commonly used instead of the secant stiffness modulus for the numerical implementation purposes. Fig. 3 schematically illustrates the advantages of using tangent stiffness modulus rather than the secant stiffness modulus. Point "A" on the stress–strain curve may follow one of the three possible paths on the stress–strain curve as shown in Fig. 3. Path (1) represents a path on which the material shows hardening behavior; the material goes to the softening region on path (2); and path (3) represents a schematic unloading path. The secant stiffness modulus of point "A" (i.e. E_A) will be the same for all these three different paths as shown in Fig. 3. However, the tangent stiffness modulus at point "A" for each of these paths will be different (i.e. $D_{A,1}$, $D_{A,2}$, and $D_{A,3}$ corresponding to paths (1), (2), and (3), respectively). Therefore, these different paths will clearly be distinguished by looking at the tangent stiffness moduli at point "A". Moreover, physically speaking, a specific area within the material at a specific time feels the tangent stiffness modulus as the instantaneous measure of its stiffness, such that a material point with a larger tangent modulus can build up more stress increment comparing to a material point with smaller tangent modulus provided that the strain increments are the same (please see Eq. (15)).

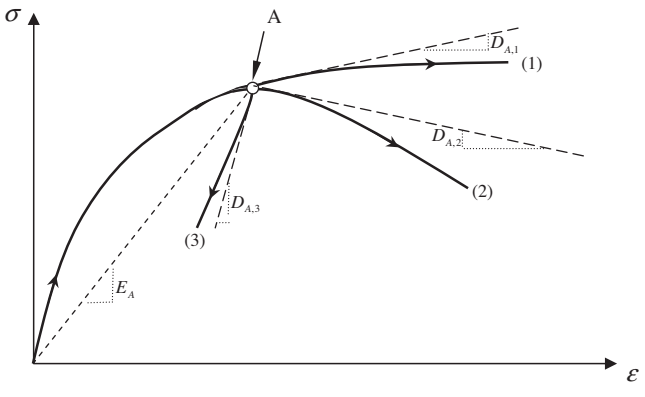

Fig. 3. Schematic illustration of three possible paths for point "A" on the stress–strain curve. Path (1) represents the path on which the material shows hardening behavior; material point goes to softening region on path (2), and path (3) represents a schematic unloading path. The secant stiffness modulus of point "A" will be the same for all these three paths. However, these paths can be distinguished by looking at the tangent stiffness modulus of point "A" for each stress–strain path.

However, one can simply derive the relationship between the tangent and secant stiffness moduli as illustrated in the following developments. For the *secant* stiffness modulus, one can write:

$$\boldsymbol{\sigma} = \boldsymbol{E} : \boldsymbol{\varepsilon} \tag{12}$$

where $\boldsymbol{E} = \boldsymbol{E}(\overline{\boldsymbol{E}}, \phi, h)$ is the fourth-order damaged-healed secant stiffness tensor, and $\boldsymbol{\varepsilon}$ is the strain tensor in the nominal configuration. Taking the time derivative of Eq. (12) yields:

$$\dot{\boldsymbol{\sigma}} = \boldsymbol{E} : \dot{\boldsymbol{\varepsilon}} + \dot{\boldsymbol{E}} : \boldsymbol{\varepsilon} = (\boldsymbol{E} + \dot{\boldsymbol{E}} : \boldsymbol{\varepsilon}\dot{\boldsymbol{\varepsilon}}^{-1}) : \dot{\boldsymbol{\varepsilon}} \tag{13}$$

The superimposed dot in this equation and all subsequent equations indicates derivative with respect to time. Also, "A^{-1}" indicates the inverse of "A". On the other hand, for the *tangent* stiffness modulus, one can write:

$$\dot{\boldsymbol{\sigma}} = \boldsymbol{D} : \dot{\boldsymbol{\varepsilon}} \tag{14}$$

The relation between the tangent and secant moduli is obtained by comparing Eqs. (13) and (14), such that:

$$\boldsymbol{D} = \boldsymbol{E} + \dot{\boldsymbol{E}} : \boldsymbol{\varepsilon}\dot{\boldsymbol{\varepsilon}}^{-1} \tag{15}$$

Different expressions for $\dot{\boldsymbol{E}}$ are derived next based on adapting three different transformation hypotheses to relate the healing configuration to the damaged configuration.

In this paper, the mechanisms such as viscoelasticity and viscoplasticity have not been considered to avoid unnecessary complexities. Therefore, derivations are presented for the elastic-damage-healing cases for simplicity. The extension of the proposed healing framework to more complex cases such as viscoelasticity and viscoplasticity will be the subject of a future work. As argued before, the stiffness moduli in the effective and healing configurations are the same (Eq. (10)) and do not change during the loading–unloading history or as the material damages or heals. Hence, one can simply imply that for elastic-damage-healing materials, the secant and tangent stiffness moduli in both effective and healing configurations are the same as the initial undamaged stiffness modulus of the intact materials, such that:

$$\overline{\boldsymbol{E}} = \overline{\overline{\boldsymbol{E}}} = \overline{\boldsymbol{D}} = \overline{\overline{\boldsymbol{D}}} \tag{16}$$

Moreover, stress and strain tensors and their rates are related through the following relationships:

$$\bar{\bar{\boldsymbol{\sigma}}} = \overline{\overline{\boldsymbol{E}}} : \bar{\bar{\boldsymbol{\varepsilon}}}; \quad \dot{\bar{\bar{\boldsymbol{\sigma}}}} = \overline{\overline{\boldsymbol{D}}} : \dot{\bar{\bar{\boldsymbol{\varepsilon}}}} \tag{17}$$

Taking the time derivative of Eq. (8) yields:

$$\dot{\boldsymbol{\sigma}} = [1 - \phi(1-h)]\dot{\bar{\bar{\boldsymbol{\sigma}}}} + (-\dot{\phi} + \dot{\phi}h + \phi\dot{h})\bar{\bar{\boldsymbol{\sigma}}} \tag{18}$$

Now, several transformation hypotheses from the healing configuration to the damage configuration are discussed. It should be noted that Eqs. (9) and (16) relate the stress tensors and stiffness moduli in the effective and healing configurations. One can also establish a general relationship between the strain tensors in the effective and healing configurations. Eq. (16) yields:

$$\overline{\boldsymbol{E}} = \overline{\overline{\boldsymbol{E}}} \Rightarrow \bar{\boldsymbol{\sigma}} : \bar{\boldsymbol{\varepsilon}}^{-1} = \bar{\bar{\boldsymbol{\sigma}}} : \bar{\bar{\boldsymbol{\varepsilon}}}^{-1} \tag{19}$$

Substituting Eq. (9) into Eq. (19) gives:

$$\bar{\boldsymbol{\varepsilon}} = \left[\frac{1 - \phi(1-h)}{1-\phi}\right]\bar{\bar{\boldsymbol{\varepsilon}}} \tag{20}$$

Eq. (20) relates the strain tensors in the effective and healing configurations and shows that these two tensors will be the same when healing is not included (i.e. $h = 0$) or when there is no damage (i.e. $\phi = 0$). Otherwise, there will be differences between the strain tensors in the effective and healing configurations depending on the levels of damage and healing. It should be noted that Eq. (20) is valid for common transformation hypotheses of the continuum damage mechanics (which will be discussed later in this work) and is independent of the postulated transformation hypothesis.

In the next sub-sections, the relationships between the strain tensors and stiffness moduli in the nominal (damaged) and healing configurations will be established for different transformation hypotheses. Relations between the stress tensors, stiffness moduli, and strain tensors in the healing and effective configurations can evidently be obtained using Eqs. (9), (16), and (20), respectively.

3.1. Strain equivalence hypothesis

The first commonly used hypothesis in CDM to relate the nominal stress and strain tensors ($\boldsymbol{\sigma}$ and $\boldsymbol{\varepsilon}$) to the stress and strain tensors in the undamaged effective configuration ($\bar{\boldsymbol{\sigma}}$ and $\bar{\boldsymbol{\varepsilon}}$) is the strain equivalence hypothesis which states that the strain tenors in the nominal and effective configurations are equal (Lemaître and Chaboche, 1990). This is the simplest transformation hypothesis that one can think about and makes the theoretical derivation and numerical implementation of constitutive models relatively easier. However, this hypothesis is inaccurate in case of large deformations and/or significant damage evolution. This hypothesis is extended here for the healing configuration such that one can assume that the strain tensors in the nominal and healing configurations are equal, such that:

$$\boldsymbol{\varepsilon} = \bar{\bar{\boldsymbol{\varepsilon}}} \quad \Rightarrow \quad \dot{\boldsymbol{\varepsilon}} = \dot{\bar{\bar{\boldsymbol{\varepsilon}}}} \tag{21}$$

It should be noted that equivalency of the strain tensors in the healing and nominal configurations does not imply the equivalency of the strain tensors in the effective and healing configurations when healing is included. In fact, Eq. (20) relates the strain tensors in the healing and effective configurations when healing is included.

Substituting Eq. (18) into $\dot{\boldsymbol{\varepsilon}} = \boldsymbol{D}^{-1} : \dot{\boldsymbol{\sigma}}$ (Eq. (14)) yields:

$$\dot{\boldsymbol{\varepsilon}} = [1-\phi(1-h)]\boldsymbol{D}^{-1} : \dot{\bar{\bar{\boldsymbol{\sigma}}}} + (-\dot{\phi} + \dot{\phi}h + \phi\dot{h})\boldsymbol{D}^{-1} : \bar{\bar{\boldsymbol{\sigma}}} \tag{22}$$

Substituting Eq. $(17)_2$ into Eq. (22) yields:

$$\dot{\boldsymbol{\varepsilon}} = [1-\phi(1-h)]\boldsymbol{D}^{\mathbf{-1}} : \overline{\overline{\boldsymbol{D}}} : \dot{\bar{\bar{\boldsymbol{\varepsilon}}}} + [-\dot{\phi} + \dot{\phi}h + \phi\dot{h}]\boldsymbol{D}^{\mathbf{-1}} : \overline{\overline{\boldsymbol{D}}} : \bar{\bar{\boldsymbol{\varepsilon}}} \tag{23}$$

Furthermore, substituting Eq. (21) into Eq. (23) gives:

$$\boldsymbol{D} = [1-\phi(1-h) + (\dot{\phi}h + \phi\dot{h} - \dot{\phi})\boldsymbol{\varepsilon} : \dot{\boldsymbol{\varepsilon}}^{-1}]\overline{\overline{\boldsymbol{D}}} \tag{24}$$

Eq. (24) expresses the changes in the nominal tangent stiffness as a function of the damage variable, the healing variable, the strain level, and their rates. As will be shown in the subsequent developments, Eq. (24) is able to capture the nonlinear response of the material during the loading as well as the unloading processes. Another feature of Eq. (24) is that it takes into account the deformation history by including the strain level. This equation can also capture the changes in the stiffness modulus at the loading–unloading point in the cyclic loading which is triggered by the presence of the strain rate in Eq. (24).

One can also simply derive the relation between the secant stiffness modulus and its rate in the nominal and healing configurations by substituting Eqs. (12), $(17)_1$, and (21) into Eq. (8), such that:

$$\boldsymbol{E} = [1-\phi(1-h)]\overline{\overline{\boldsymbol{E}}} \tag{25}$$

Taking the time derivative of Eq. (25) and noting that the secant modulus in the healing configuration is constant (i.e. $\dot{\overline{\overline{\boldsymbol{E}}}} = 0$) imply:

$$\dot{\boldsymbol{E}} = (-\dot{\phi} + \dot{\phi}h + \phi\dot{h})\overline{\overline{\boldsymbol{E}}} \tag{26}$$

Eqs. (25) and (26) relate the secant stiffness modulus and its rate in the nominal configuration to their corresponding counterparts in the healing configuration. It should be noted that Eq. (24) can be derived simply by substituting Eqs. (16), (25), and (26) into Eq. (15).

3.2. Elastic strain energy equivalence hypothesis

Another commonly used transformation hypothesis in CDM is the elastic strain energy equivalence hypothesis (Cordebois and Sidoroff, 1982; Voyiadjis and Kattan, 1993; Lemaître et al., 2000), which is more physically sound comparing to the strain equivalence hypothesis (Abu Al-Rub and Voyiadjis, 2003). The elastic strain energy densities in the nominal and healing configurations for the elastic-damage-healing materials can be written as follows:

$$W = \frac{1}{2}\boldsymbol{\sigma} : \boldsymbol{\varepsilon}; \quad \overline{\overline{W}} = \frac{1}{2}\bar{\bar{\boldsymbol{\sigma}}} : \bar{\bar{\boldsymbol{\varepsilon}}} \tag{27}$$

The elastic strain energy equivalence hypothesis states that the elastic strain energy densities in the nominal and effective configurations are the same (i.e. the elastic strain energy is stored in the intact material). This hypothesis is postulated here for the nominal and healing configurations, such that:

$$W = \overline{\overline{W}} \tag{28}$$

However, this hypothesis does not imply the equivalency of the elastic strain energy in the nominal and effective configurations when healing is included. The relationship between the elastic strain energies in the effective, nominal, and healing configurations can be obtained using Eqs. (9), (20), and (28), such that:

$$W = \overline{\overline{W}} = \left[\frac{1-\phi}{1-\phi(1-h)}\right]^2 \overline{W} \tag{29}$$

where $\overline{W} = \bar{\boldsymbol{\sigma}} : \bar{\boldsymbol{\varepsilon}}/2$. Eq. (29) shows that the elastic strain energy in the effective configuration will be equivalent to that in the nominal and healing configurations only when the healing variable is zero (i.e. healing is not included) or when there is no damage. Substituting Eqs. (8) and (27) into Eq. (28) yields:

$$\bar{\bar{\boldsymbol{\varepsilon}}} = [1-\phi(1-h)]\boldsymbol{\varepsilon} \tag{30}$$

Eq. (30) relates the strain tensors in the nominal and healing configurations. The relationship between the tangent moduli in the nominal and healing configurations can then be obtained by substituting Eqs. (12), (14), (16), (17), and (30) into Eq. (18), such that:

$$\boldsymbol{D} = \{[1-\phi(1-h)]^2 + 2(-\dot{\phi} + \dot{\phi}h + \phi\dot{h})[1-\phi(1-h)]\boldsymbol{\varepsilon} : \dot{\boldsymbol{\varepsilon}}^{-1}\}\overline{\overline{\boldsymbol{D}}} \tag{31}$$

Furthermore, the relations between the secant stiffness modulus and its rate in the nominal and healing configurations can be derived by substituting Eqs. (12), (16), $(17)_1$, and (30) into Eq. (8), such that:

$$\boldsymbol{E} = [1-\phi(1-h)]^2\overline{\overline{\boldsymbol{E}}} \tag{32}$$

$$\dot{\boldsymbol{E}} = 2(-\dot{\phi} + \dot{\phi}h + \phi\dot{h})[1-\phi(1-h)]\overline{\overline{\boldsymbol{E}}} \tag{33}$$

Equivalently, substituting Eqs. (32) and (33) into Eq. (15) confirms Eq. (31).

3.3. Power equivalence hypothesis

Another transformation hypothesis to relate strains and stiffness moduli in the nominal and effective configurations in the absence of micro-damage healing is the power equivalence hypothesis. This hypothesis has been used by several researchers

to derive constitutive models associated with dissipative processes such as viscoelasticity and viscoplasticity. To name a few, Lee et al. (1985), Voyiadjis and Thiagarajan (1997), and Voyiadjis et al. (2004) used this hypothesis to couple damage to plasticity and/or viscoplasticity models. This hypothesis is extended here to the healing configuration (instead of the effective configuration) such that one can assume that the power expenditures in the nominal and healing configurations are the same. This hypothesis is attractive for mechanisms associated with dissipation processes since the correct estimation of the dissipated energy is generally needed. It is noteworthy that using the power equivalence hypothesis along with the concept of the stress in the healing configuration is both numerically and physically interesting. Using the concept of the stress in the healing configuration eliminates numerical complexities associated with direct coupling between the damage and healing constitutive equations and at the same time makes these simplifications physically sound since it allows the accurate estimation of the dissipated energy in the healing configuration.

The power expenditures in the nominal and healing configurations can be written as:

$$\Pi = \frac{1}{2}\boldsymbol{\sigma} : \dot{\boldsymbol{\varepsilon}}; \quad \overline{\overline{\Pi}} = \frac{1}{2}\bar{\bar{\boldsymbol{\sigma}}} : \dot{\bar{\bar{\boldsymbol{\varepsilon}}}} \tag{34}$$

Power equivalence hypothesis states that the power expenditure in the nominal, Π, and healing, $\overline{\overline{\Pi}}$, configurations are the same, such that:

$$\Pi = \overline{\overline{\Pi}} \tag{35}$$

Substituting Eqs. (8) and (34) into Eq. (35) yields:

$$\dot{\bar{\bar{\boldsymbol{\varepsilon}}}} = [1-\phi(1-h)]\dot{\boldsymbol{\varepsilon}} \tag{36}$$

which relates the rate of the nominal strain tensor to its rate in the healing configuration. Substituting $\boldsymbol{\sigma}$ from Eq. (8) along with $\dot{\boldsymbol{\varepsilon}}$ from Eq. (14) into Eq. $(34)_1$ gives:

$$\Pi = \frac{1}{2}[1-\phi(1-h)]\bar{\bar{\boldsymbol{\sigma}}} : \boldsymbol{D}^{-1} : \dot{\boldsymbol{\sigma}} \tag{37}$$

Substituting Eqs. (16), $(17)_2$, and (18) into Eq. (37) gives:

$$\begin{aligned}\Pi = {} & \frac{1}{2}[1-\phi(1-h)]^2\bar{\bar{\boldsymbol{\sigma}}} : \boldsymbol{D}^{-1} : \overline{\overline{\boldsymbol{D}}} \\ & : \dot{\bar{\bar{\boldsymbol{\varepsilon}}}} + \frac{1}{2}[1-\phi(1-h)](-\dot{\phi}+\dot{\phi}h+\phi\dot{h})\bar{\bar{\boldsymbol{\sigma}}} : \boldsymbol{D}^{-1} : \overline{\overline{\boldsymbol{D}}} : \bar{\bar{\boldsymbol{\varepsilon}}}\end{aligned} \tag{38}$$

Using the power equivalence hypothesis (Eq. (35)) along with Eqs. (34) and (38), one obtains the following expression for the tangent moduli:

$$D = \{[1-\phi(1-h)]^2 + [1-\phi(1-h)](-\dot{\phi}+\dot{\phi}h+\phi\dot{h})\bar{\bar{\boldsymbol{\varepsilon}}} : \dot{\bar{\bar{\boldsymbol{\varepsilon}}}}^{-1}\}\overline{\overline{\boldsymbol{D}}} \tag{39}$$

The expressions in Eqs. (24), (31), and (39) show different relations between the tangent moduli in the nominal and healing configurations when different transformation hypotheses are postulated. Note that the right-hand-side of Eq. (39) is expressed as a function of the strain tensor, $\bar{\bar{\boldsymbol{\varepsilon}}}$, and its rate, $\dot{\bar{\bar{\boldsymbol{\varepsilon}}}}$, in the healing configuration. One may still represent the right-hand-side of Eq. (39) as a function of the strain tensor in the nominal configuration by using Eq. (36), such that:

$$\bar{\bar{\boldsymbol{\varepsilon}}} = \int_0^t [1-\phi(1-h)]\dot{\boldsymbol{\varepsilon}}dt \tag{40}$$

Applying the integration by parts to Eq. (40) implies:

$$\bar{\bar{\boldsymbol{\varepsilon}}} = [1-\phi(1-h)]\boldsymbol{\varepsilon} - \int_0^t (-\dot{\phi}+\dot{\phi}h+\phi\dot{h})\boldsymbol{\varepsilon}dt \tag{41}$$

Eqs. (30) and (41) show that postulating the power equivalence hypothesis yields a more general relationship between the strain tensors in the nominal and healing configurations as compared to the relations obtained by postulating the elastic strain energy or strain equivalence hypotheses. The difference between Eqs. (30) and (41) will be negligible for very slow processes where rate of the healing and damage variables are close to zero. Otherwise, there will be significant difference between these two expressions. Eq. (39) can now be expressed in terms of the nominal strain tensor by substituting Eqs. (36) and (41) into Eq. (39), such that:

$$\begin{aligned}D = {} & \Big\{[1-\phi(1-h)]^2 + \boldsymbol{\varepsilon} : \dot{\boldsymbol{\varepsilon}}^{-1}[1-\phi(1-h)](-\dot{\phi}+\dot{\phi}h+\phi\dot{h}) \\ & -(-\dot{\phi}+\dot{\phi}h+\phi\dot{h})\left[\int_0^t (-\dot{\phi}+\dot{\phi}h+\phi\dot{h})\boldsymbol{\varepsilon}dt\right] : \dot{\boldsymbol{\varepsilon}}^{-1}\Big\}\overline{\overline{\boldsymbol{D}}}\end{aligned} \tag{42}$$

Furthermore, the relationship between the secant stiffness moduli in the nominal and healing configurations can be obtained by substituting Eqs. (12), $(17)_1$, and (41) into Eq. (8), such that:

$$\boldsymbol{E} = \left\{[1-\phi(1-h)]^2 - [1-\phi(1-h)]\left[\int_0^t (-\dot{\phi}+\dot{\phi}h+\phi\dot{h})\boldsymbol{\varepsilon}dt\right] : \dot{\boldsymbol{\varepsilon}}^{-1}\right\}\overline{\overline{\boldsymbol{E}}} \tag{43}$$

Moreover, taking the time derivative of Eq. (43) yields:

$$\begin{aligned}\dot{\boldsymbol{E}} = {} & \Big\{[1-\phi(1-h)](-\dot{\phi}+\dot{\phi}h+\phi\dot{h}) - (-\dot{\phi}+\dot{\phi}h+\phi\dot{h}) \\ & \times \left[\int_0^t (-\dot{\phi}+\dot{\phi}h+\phi\dot{h})\boldsymbol{\varepsilon}dt\right] : \boldsymbol{\varepsilon}^{-1}[1-\phi(1-h)] \\ & \times \left[\int_0^t (-\dot{\phi}+\dot{\phi}h+\phi\dot{h})\boldsymbol{\varepsilon}dt\right] : \boldsymbol{\varepsilon}^{-1} : \dot{\boldsymbol{\varepsilon}} : \boldsymbol{\varepsilon}^{-1}\Big\}\overline{\overline{\boldsymbol{E}}}\end{aligned} \tag{44}$$

Eqs. (39) and (42) show the expressions for relating the damaged (nominal) tangent stiffness modulus to the stiffness of the intact material as a function of the damage density, healing variable, strain, and their rates. These relations can be used to capture the nonlinear change in the stiffness during the unloading since during the unloading both the strain and the healing variable change. Furthermore, the presence of the strain rate enriches Eqs. (24), (31), and (39) to capture the changes in the stiffness modulus of the loading–unloading point in the cyclic loading. These important features of these equations will be shown in the following section in order to show the capabilities of the model in cyclic loading.

4. Damage and healing evolution functions

Several examples are presented in this section to show the capabilities of the proposed micro-damage healing framework in capturing the nonlinear response of materials under cyclic loading. Recently, Darabi et al. (2011a) and Abu Al-Rub et al. (2010) have proposed and validated rate-dependent damage (viscodamage or delay-damage) and healing models, respectively, and coupled those to viscoelasticity and viscoplasticity constitutive models to predict the mechanical response of bituminous materials. A general thermodynamic framework for constitutive modeling of the damage and micro-damage healing processes in self-healing materials is presented in the Appendix. Also, in the Appendix, the proposed thermodynamic framework is used to derive the constitutive models of Darabi et al. (2011a) and Abu Al-Rub et al. (2010).

The rate-dependent damage model (viscodamage) of Darabi et al. (2011a) can be written as follows:

$$\dot{\phi} = \Gamma^{vd}\left(\frac{\overline{\overline{Y}}}{Y_{th}}\right)^q (1-\phi)^2 \exp(k\bar{\bar{\boldsymbol{\varepsilon}}}_{eff}) \tag{45}$$

where Γ^{vd} is the viscodamage viscosity parameter that controls how fast damage nucleates and grows; k and q are model parame-

ters; $\bar{\bar{\varepsilon}}_{eff} = \sqrt{\bar{\bar{\varepsilon}}_{ij}\bar{\bar{\varepsilon}}_{ij}}$ is the effective (or equivalent) strain; Y_{th} is the threshold damage force; and $\bar{\bar{Y}}$ is the damage driving force which has the extended Drucker–Prager form, such that:

$$\bar{\bar{Y}} = \bar{\bar{\tau}}^{vd} - \alpha \bar{\bar{I}}_1 \tag{46}$$

where $\bar{\bar{\tau}}^{vd}$ is the deviatoric component of the damage force in the healing configuration, such that:

$$\bar{\bar{\tau}}^{vd} = \frac{\sqrt{3\bar{\bar{J}}_2}}{2}\left[1 + \frac{1}{d^{vd}} + \left(1 - \frac{1}{d^{vd}}\right)\frac{3\bar{\bar{J}}_3}{\sqrt{3\bar{\bar{J}}_2^3}}\right] \tag{47}$$

where d^{vd} is a material parameter which gives the distinction of the material's damage response in compressive and extensive loading conditions; $\bar{\bar{J}}_2 = \frac{1}{2}\bar{\bar{s}}_{ij}\bar{\bar{s}}_{ij}$ and $\bar{\bar{J}}_3 = \frac{1}{2}\bar{\bar{s}}_{ij}\bar{\bar{s}}_{jk}\bar{\bar{s}}_{ki}$ are the second and the third deviatoric stress invariants with $\bar{\bar{s}}_{ij} = \bar{\bar{\sigma}}_{ij} - \frac{1}{3}\bar{\bar{\sigma}}_{kk}\delta_{ij}$ being the deviatoric stress and δ_{ij} being the Kronecker delta.

Darabi et al. (2011a,b) coupled this viscodamage model to the Schapery's (1969)viscoelasticity model and Perzyna's (1971) viscoplasticity model and successfully validated the model against an extensive experimental data on bituminous materials including creep, constant strain rate, and single creep-recovery tests at various temperatures, stress levels, and strain rates in both tension and compression. The model showed reasonable predictions with the experimental measurements. However, the model underestimated the number of loading cycles up to failure for the repeated creep-recovery tests when relatively long rest periods were introduced between the loading cycles. The reason for this underestimation was related to micro-damage healing occurring during the unloading time or the rest period (see e.g.Kim and Little, 1990; Little and Bhasin, 2007; Bhasin et al., 2008). To remedy this issue, Abu Al-Rub et al. (2010) proposed a simple phenomenological-based healing model which can be written as follows:

$$\dot{h} = \Gamma^h(1-\phi)^{m_1}(1-h)^{m_2} \tag{48}$$

where Γ^h is the healing viscosity parameter controlling the rate of the micro-damage healing, and m_1 and m_2 are model material parameters.

It was shown that consideration of micro-damage healing significantly improves the predictions of the repeated creep-recovery tests in both tension and compression. The repeated uniaxial creep-recovery tests in compression were conducted for different loading/unloading times when the applied stress level was 1500 kPa. Fig. 4 shows the model predictions with and without considering micro-damage healing for the uniaxial repeated creep-recovery tests for different loading/unloading times.

Fig. 4(a)–(c) show that as the rest period increases, the model predictions without the micro-damage healing significantly underestimates the experimental measurements. The reason is that more micro-cracks can heal as the rest period increases. On the other hand, once the micro-damage healing is considered, the model predictions agree well with the experimental measurements. Model predictions for the uniaxial repeated creep-recovery tests in tension are also presented in Fig. 5. Fig. 5 also shows the capability of the micro-damage healing model in capturing the experimental measurements in the presence of the rest periods.

Figs. 4 and 5 show the model capabilities in capturing the effect of micro-damage healing on the mechanical response of materials (please refer to Abu Al-Rub et al. (2010) for more details).

It should be noted that these constitutive models for the damage and micro-damage healing should be regarded as simplified illustrations and not full-fledged constitutive models. Although the main goal of this paper is not to compare with experimental measurements, specific damage and micro-damage healing models

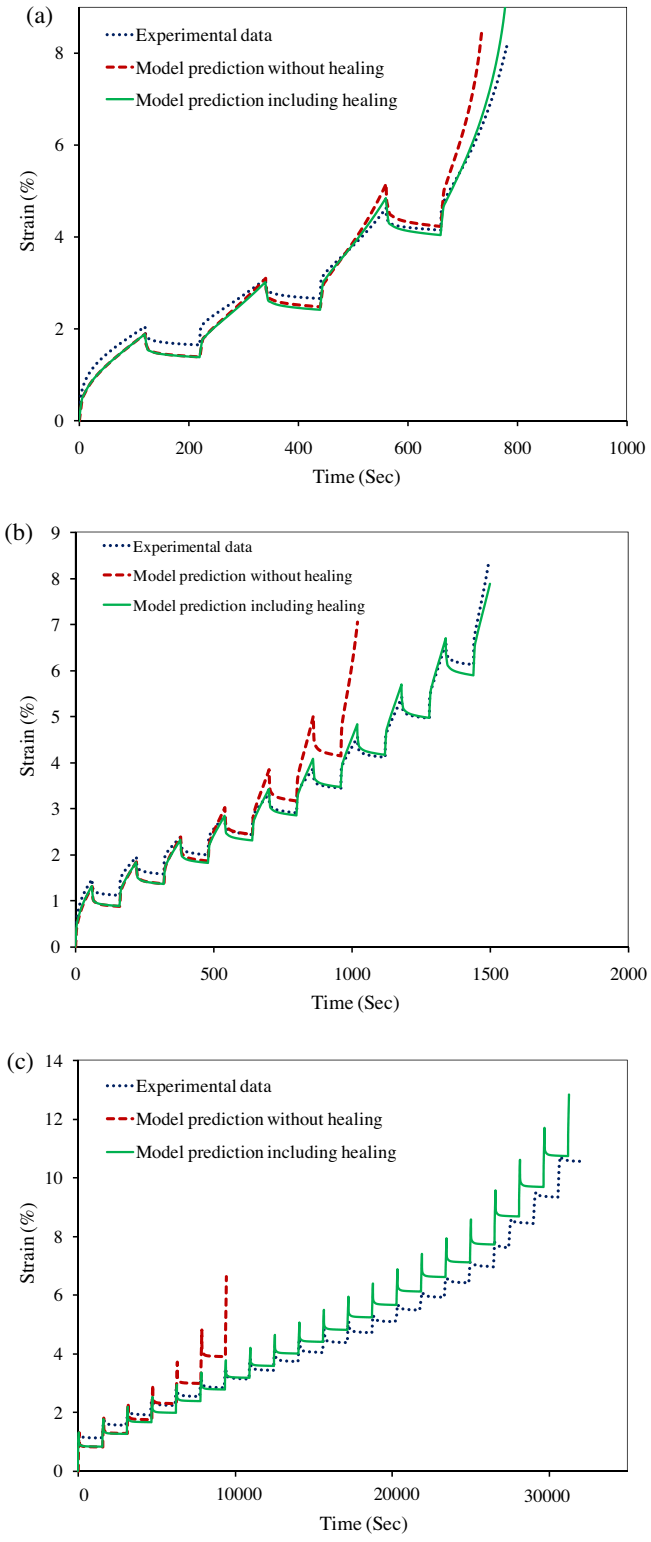

Fig. 4. Experimental data and model predictions with and without micro-damage healing model for the uniaxial repeated creep-recovery tests in compression for different loading times (LT) and unloading times (UT) when the applied stress is 1500 kPa and temperature is 20 °C. (a) LT = 120 s and UT = 100 s; (b) LT = 60 s and UT = 100 s; (c) LT = 60 s and UT = 1500 s.

that have been validated thoroughly are selected in order to show the characteristics of the proposed general framework.

The main objective of this study is to investigate the qualitative effect of the damage and micro-damage healing models on mechanical response of materials. Therefore, to avoid unnecessary

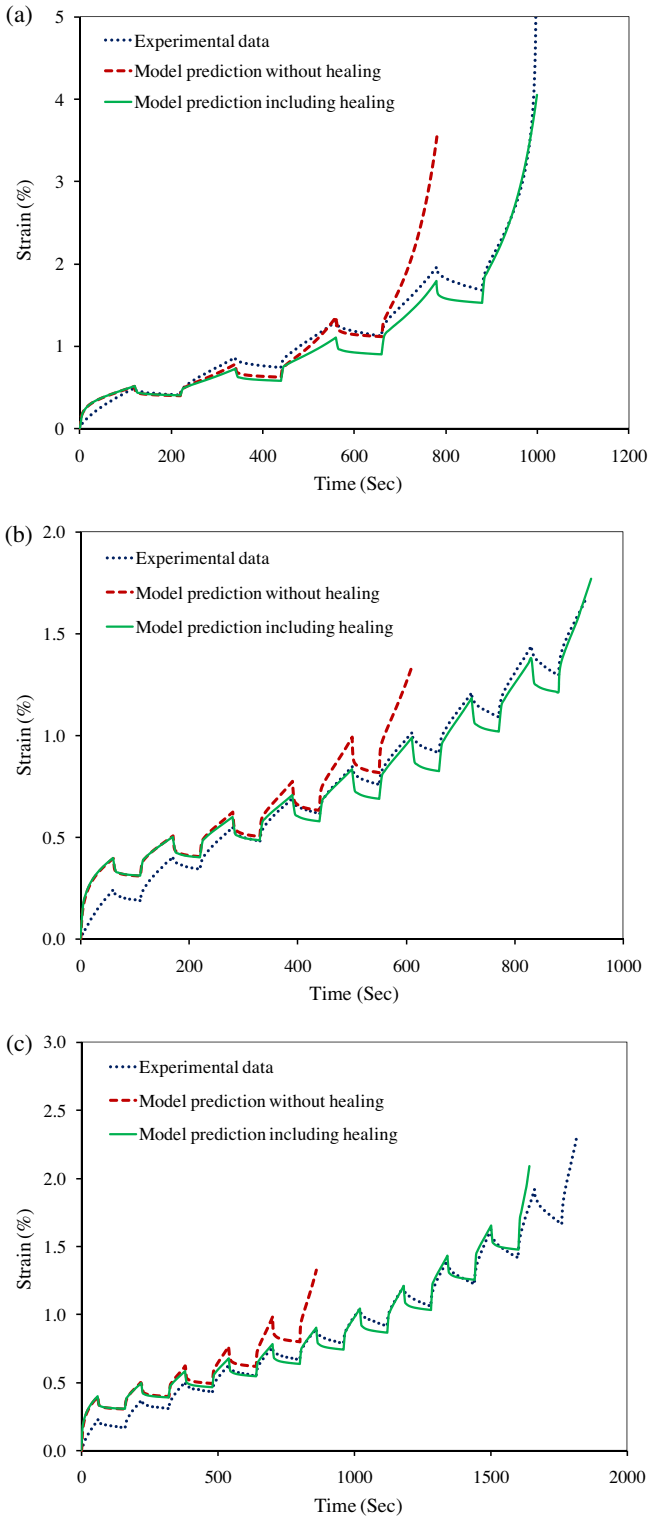

Fig. 5. Experimental data and model predictions with and without micro-damage healing model for the uniaxial repeated creep-recovery tests in tension for different loading times (LT) and unloading times (UT) when the applied stress is 300 kPa and temperature is 20 °C. (a) LT = 120 s and UT = 100 s; (b) LT = 60 s and UT = 50 s; (c) LT = 60 s and UT = 100 s.

complexities, simplified versions of the presented damage and micro-damage healing models are considered in this work. The simplified form of the viscodamage model which is used in this work can be written as follows:

$$\dot{\phi} = \Gamma^{vd}\left(\frac{\overline{\overline{Y}}}{Y_{th}}\right)(1-\phi)^2\exp(k\bar{\bar{\varepsilon}}_{eff}); \quad \overline{\overline{Y}} = \sqrt{3\bar{\bar{J}}_2} \tag{49}$$

The presented viscodamage model in Eq. (49) can be treated analogously to viscoplasticity models such that the damage variable evolves when the material state is on or outside the viscodamage loading surface. The viscodamage loading surface can be simply extracted from the damage evolution function in Eq. (49) as follows:

$$f^{vd} = \frac{\overline{\overline{Y}}}{Y_{th}}(1-\phi)^2\exp(k\bar{\bar{\varepsilon}}_{eff}) - \frac{\dot{\phi}}{\Gamma^{vd}} \leqslant 0 \tag{50}$$

where f^{vd} is the viscodamage loading surface. Hence, the damage variable ϕ evolves when the viscodamage surface is equal or greater than zero.

Moreover, the simplified form of the micro-damage healing model which is used in this work can be written as follows:

$$\dot{h} = \Gamma^{h}[(1-\phi)(1-h)]^m \tag{51}$$

The following initiation condition was also postulated for the healing model:

$$f^{h} = \bar{\bar{\varepsilon}}^{h}_{th} - \bar{\bar{\varepsilon}}_{eff} \leqslant 0 \tag{52}$$

where f^h is the healing loading surface, $\bar{\bar{\varepsilon}}^{h}_{th}$ is the healing threshold strain, and $\bar{\bar{\varepsilon}}_{eff}$ is the effective strain. Eq. (52) assumes that the healing variable evolves when the total effective strain is smaller than the healing threshold strain. In other words, the healing occurs at very small strains such that the micro-crack faces are close to each other and can wet each other in order for healing to occur. Moreover, it should be noted that healing cannot occur during the damage process and vice versa (i.e. a micro-crack cannot propagate and heal at the same time; either propagates or heals). Hence, the rate of healing will be zero when damage is evolving (i.e. when $\dot{\phi} \geqslant 0$).

In the following subsections, the effect of assuming rate-dependent damage versus rate-independent damage on the mechanical responses will also be investigated. Therefore, the following function is assumed to describe the rate-independent damage model, such that:

$$\phi = \gamma\left(\frac{\overline{\overline{Y}}}{Y_{th}}\right)\exp(k\bar{\bar{\varepsilon}}_{eff}) \tag{53}$$

The main difference between Eqs. (49) and (53) is that the former is time- and rate-dependent which considers the loading time as well as the loading rate while the later is time- and rate-independent.

It is noteworthy that the presented models will be used to show qualitative effects of damage and healing on the mechanical response of elastic-damage-healing materials. Obviously, the evolution functions for the damage and healing models can be different for different materials, but similar qualitative trends will be obtained by following the above formulated continuum damage mechanics framework considering micro-damage healing.

5. Numerical implementation procedure for different transformation hypotheses

The implementation procedure for the presented elastic-damage-healing model using different transformation hypotheses is discussed in this subsection. However, as it will be discussed, the implementation procedure is general and independent of the selected evolution functions for the damage and healing models.

The use of the concept of the stress in the healing configurations substantially simplifies the numerical implementation of the damage and healing models, especially, for complex constitutive models where damage and healing models are coupled to

viscoelasticity and/or viscoplasticity models. In other words, one can update the stress tensor in the healing configuration $\bar{\bar{\boldsymbol{\sigma}}}^{t+\Delta t}$ without facing the complexities associated with the direct couplings of the damage and healing models to the rest of the constitutive model. The updated stress in the healing configuration can then be used to update the damage and healing variables and subsequently the nominal stress tensor. It should be noted that the nominal strain increment tensor $\Delta\boldsymbol{\varepsilon}^{t+\Delta t}$as well as the nominal total strain tensor $\boldsymbol{\varepsilon}^{t+\Delta t}$ at the current time $t+\Delta t$ are given at the beginning of each increment. The nominal strain tensor and its increment will be the same as those in the healing configuration if the strain equivalence hypothesis is used. However, the nominal strain tensor and its increment will be different from their corresponding values in the healing configuration if either the elastic strain energy equivalence or the power equivalence hypotheses are used. Therefore, an iterative scheme is needed to obtain the total strain and the strain increment tensors in the healing configuration at time $t+\Delta t$ when the elastic strain energy equivalence or power equivalence hypotheses are used. The total nominal strain tensor and its increment at the current time $t+\Delta t$, the values of the internal state variables (i.e. ϕ, h, and ϕ_{eff}) at previous time t, and the stress tensors in the nominal and healing configurations at previous time t are known. The objective is to update the current stress tensors in the nominal and healing configurations as well as the strain tensor in the healing configuration at the current time $t+\Delta t$. Hence, one can start with a trial strain tensor in the healing configuration when the elastic strain energy equivalence hypothesis is used, such that:

$$\bar{\bar{\boldsymbol{\varepsilon}}}^{tr,t+\Delta t} = \left(1-\phi^{t}_{eff}\right)\boldsymbol{\varepsilon}^{t+\Delta t} \tag{54}$$

Similarly, one can start with a trial strain increment in the healing configuration when the power equivalence hypothesis is used, such that:

$$\Delta\bar{\bar{\boldsymbol{\varepsilon}}}^{tr,t+\Delta t} = \left(1-\phi^{t}_{eff}\right)\Delta\boldsymbol{\varepsilon}^{t+\Delta t} \tag{55}$$

Subsequently, the total trial strain tensor in the healing configuration can be obtained for the power equivalence hypothesis (using Eq. (55)), such that:

$$\bar{\bar{\boldsymbol{\varepsilon}}}^{tr,t+\Delta t} = \bar{\bar{\boldsymbol{\varepsilon}}}^{t} + \Delta\bar{\bar{\boldsymbol{\varepsilon}}}^{tr,t+\Delta t} \tag{56}$$

The trial strain in the healing configuration (Eq. (54)) for the elastic strain energy equivalence hypothesis; Eqs. (55) and (56) for the power equivalence hypothesis] can then be fed to Hooke's law (Eq. (17)) to update the stress in the healing configuration. The next step is to calculate the damage and healing variables based on the obtained trial strain and stress tensors in the healing configuration. In this step, the damage force in the healing configuration (i.e. $\bar{\bar{Y}}$) and the strain tensor in the healing configuration (i.e. $\bar{\bar{\boldsymbol{\varepsilon}}}$) are constant. Therefore, one can start with the trial value for the viscodamage surface, Eq. (50), such that:

$$f^{vd,tr} = \frac{\bar{\bar{Y}}}{Y_{th}}(1-\phi^{t})^{2}\exp(k\bar{\bar{\boldsymbol{\varepsilon}}}_{eff}) - \frac{\Delta\phi^{t}}{\Gamma^{vd}\Delta t} \tag{57}$$

The damage increment can now be obtained using the Newton–Raphson scheme. However, the differential of the f^{vd} with respect to $\Delta\phi$ is needed which can be expressed as follows:

$$\frac{\partial f^{vd}}{\partial\Delta\phi} = -\frac{\bar{\bar{Y}}}{Y_{th}}(1-\phi)\exp(k\bar{\bar{\boldsymbol{\varepsilon}}}_{eff}) - \frac{1}{\Gamma^{vd}\Delta t} \tag{58}$$

Hence, the damage density increment at the $k+1$ iteration can be obtained as follows:

$$(\Delta\phi^{t+\Delta t})^{k+1} = (\Delta\phi^{t+\Delta t})^{k} - \left[\left(\frac{\partial f^{vd}}{\partial\Delta\phi^{t+\Delta t}}\right)^{k}\right]^{-1} f^{vd} \tag{59}$$

The damage density can then be obtained, such that:

$$\phi^{t+\Delta t} = \phi^{t} + \dot{\phi}^{t+\Delta t}\Delta t \tag{60}$$

The same procedure can be applied to calculate the healing variable. In other words, the rate of the healing variable $\dot{h}^{t+\Delta t}$ (if the healing criterion is met) should be calculated first using Eq. (51). However, as mentioned earlier, healing does not occur during the damage process and vice versa. Hence, the healed area A^{h} remains constant during the damage evolution. However, during the healing process both the healing area A^{h} and the total damage area $A^{D} = A^{h} + A^{uh}$ which is the summation of the healed and unhealed damage areas evolve. Taking the time derivative of Eq. (5) and making use of Eq. (4) yield the following relations for the updated healing variable:

$$\begin{cases} h^{t+\Delta t} = \frac{\phi^{t}}{\phi^{t+\Delta t}}h^{t}; & \dot{\phi}^{t+\Delta t} \geqslant 0 \\ h^{t+\Delta t} = h^{t} + \dot{h}^{t+\Delta t}\Delta t; & \dot{\phi}^{t+\Delta t} = 0 \end{cases} \tag{61}$$

The new trial strain tensor in the healing configuration will then be recalculated using updated damage and healing variables. At the end of the iteration, the new and old values of the strain tensor in the healing configuration will be compared to check the convergence. Fig. 6 shows the flowchart for implementation of the presented elastic-damage-healing constitutive model using different transformation hypotheses.

6. Numerical results and examples

The presented elastic-damage-healing model is implemented in the well-known commercial finite element code Abaqus (2008) via the user material subroutine UMAT. The finite element model considered here is simply a three-dimensional single element (C3D8R) available in Abaqus.

6.1. Example 1: different transformation hypotheses

The effect of postulating different transformation hypotheses on the mechanical responses is investigated in this subsection. The rate-dependent damage and healing models (Eqs. (45) and (48)) along with the model parameters listed in Table 1 are used for the examples presented in this section.

The first simulated example is the uniaxial constant strain rate test (i.e. strain-controlled uniaxial test). The strain rate is selected as 0.005/sec. The loading history for this test is shown in Fig. 7(a). Therefore, during this numerical test, no healing is expected. The stress–strain responses using different transformation hypotheses are shown in Fig. 7(b). Fig. 7(b) shows that the response of all transformation hypotheses is close to each other at small strains. However, these responses deviate when the strain and subsequently the damage density increase. Fig. 7(b) shows different responses for the peak point of the stress–strain diagram and the post peak region in the stress–strain diagram when different transformation hypotheses are postulated. Furthermore, it shows that the stress–strain response using the power equivalence hypothesis lies between the numerical results from the strain equivalence and elastic strain energy equivalence hypotheses. The ratio of the elastic strain energy and the expended power in the healing configuration to their corresponding values in the nominal configuration for different transformation hypotheses are plotted in Fig. 7(c) and (d), respectively. Fig. 7(c) shows that both the strain equivalence and power equivalence hypotheses predict higher values for the elastic strain energy in the healing configuration comparing to their corresponding values in the nominal configuration. However, this

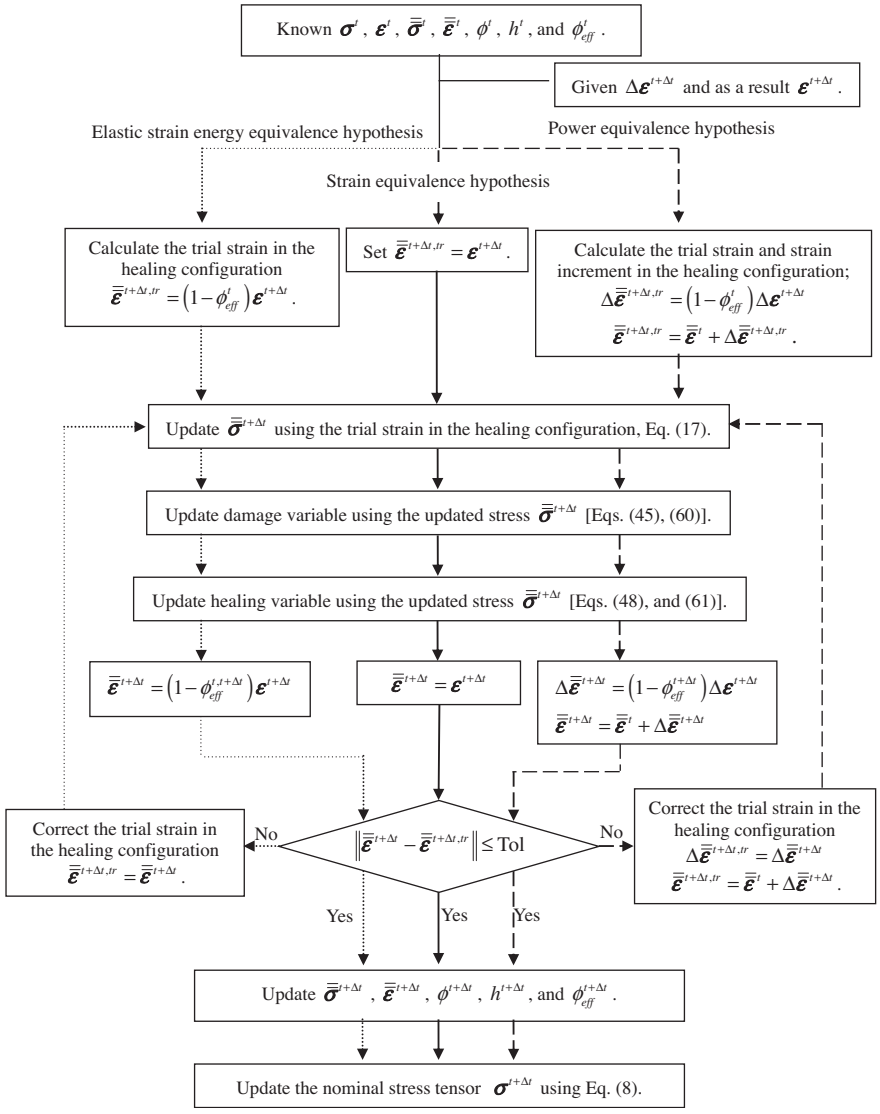

Fig. 6. A flowchart showing the general finite element implementation procedure of the elastic-damage-healing model using different transformation hypotheses.

Table 1
Model parameters associated with the presented elastic-damage-healing constitutive model.

$\bar{\bar{\boldsymbol{E}}}$ (GPa)	v	γ	Γ^{vd} (s^{-1})	k	Y_{th} (MPa)	Γ^h (s^{-1})	m	$\bar{\varepsilon}_{th}^h$
2	0.25	0.25	5×10^{-7}	75	2	0.03	2	0.001

deviation is more significant when the strain equivalence hypothesis is used. On the other hand, Fig. 7(d) shows that the strain equivalence hypothesis predicts larger values for the expended power in the healing configuration comparing to its corresponding value in the nominal configuration; whereas, the elastic energy equivalence hypothesis predicts lower values for the expended power in the healing configuration comparing to that in the nominal configuration. However, it should be noted that the main purpose of using the fictitious healing and/or effective configurations along with a specific transformation hypothesis is to make the implementation simpler while the underlying physics is preserved. Also, a proper transformation hypothesis is a one that leads to a constitutive model that is equivalent when expressed in both the nominal and healing configurations since both configurations are tools to represent the same material behavior. It is also interesting to look at this problem from the thermodynamic point of view. As stated by Ziegler (1977) and have used by many other researchers (Coleman and Gurtin, 1967; Rice, 1971; Ziegler, 1983; Ziegler and Wehrli, 1987; Fremond and Nedjar, 1996; Collins and Houlsby, 1997; Shizawa and Zbib, 1999) the constitutive equations for a material are fully determined by the knowledge of the Helmholtz free energy and a dissipation function such as the rate of the energy dissipation. Therefore, two systems will be thermodynamically equivalent if they predict equivalent responses for an energetic function such as the stored energy and for a dissipative function such as dissipated power. As shown in Fig. 5(c) and (d), none of these hypotheses predict the same value for both of these two energetic measures (i.e. strain energy and energy power) functions in nominal and healing configurations. Therefore, qualitative investigation of the responses of each transformation hypothesis is extremely important in deciding the properness of a specific transformation hypothesis for a specific type of material. For example, one can use the strain equivalence hypothesis for simplicity if the damage density is expected to be low. On the other hand, one may use the elastic energy equivalence hypothesis for the brittle materials for which the elastic strain energy can be considered as the driving force for damage nucleation and growth. Finally, the

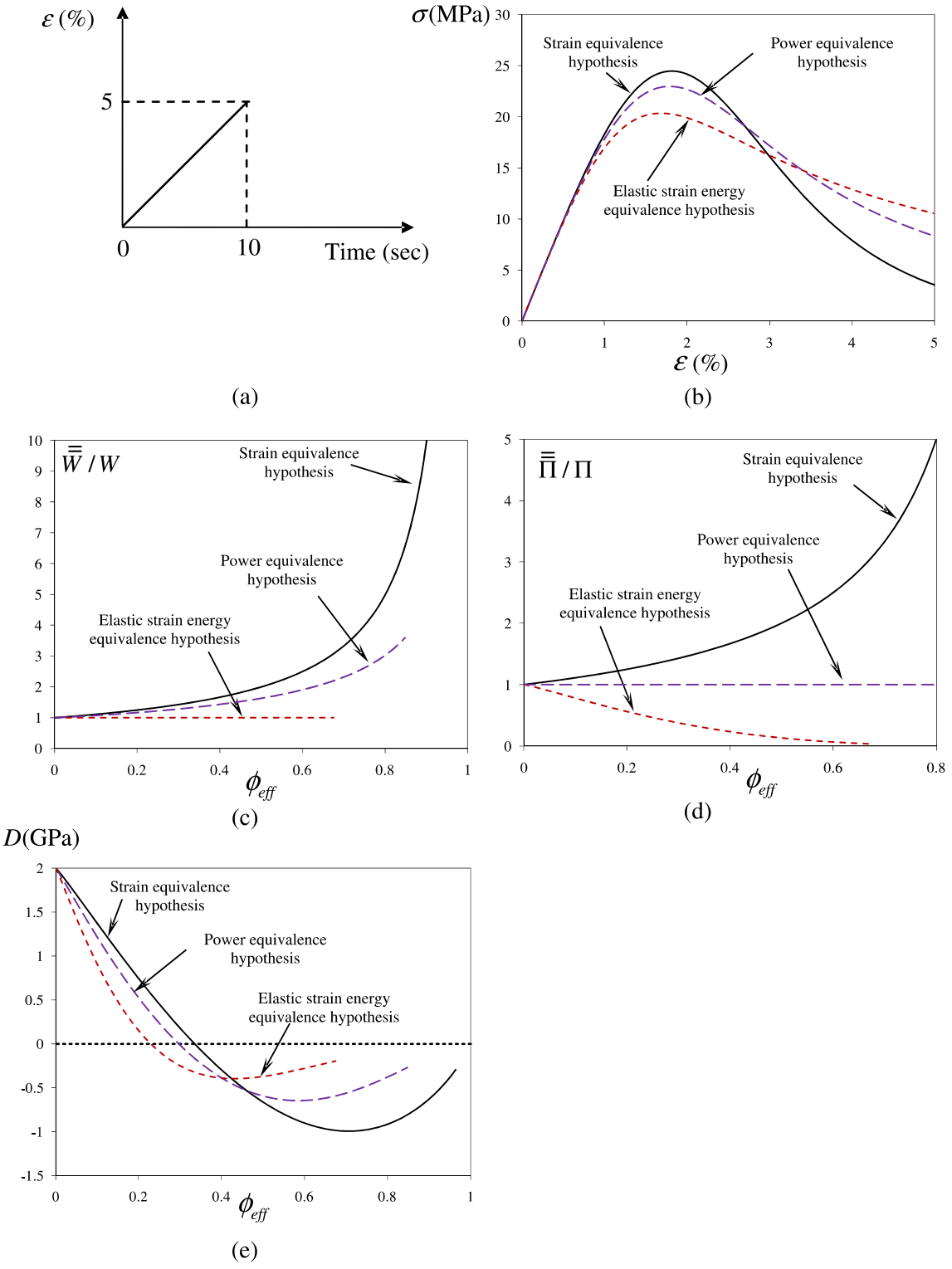

Fig. 7. Model predictions for a uniaxial constant strain rate test using different transformation hypothesis. (a) Loading history; (b) stress–strain responses; (c) ratio of the elastic strain energy in the healing configuration over that in the nominal configuration; (d) ratio of the expended power in the healing configuration over that in the nominal configuration; and (e) tangent stiffness moduli.

power equivalence hypothesis could be used for complex constitutive models including viscoelasticity and viscoplasticity in which case the elastic strain energy is negligible comparing to the total strain energy and also the dissipative power and energy becomes of great interest. Appendix presents a general thermodynamic framework for constitutive modeling of damage and micro-damage healing mechanisms. This proposed thermodynamic framework is in line with the key assumption of Ziegler's work since it only needs the information of the Helmholtz free energy and rate of the energy dissipation to derive the constitutive models. This

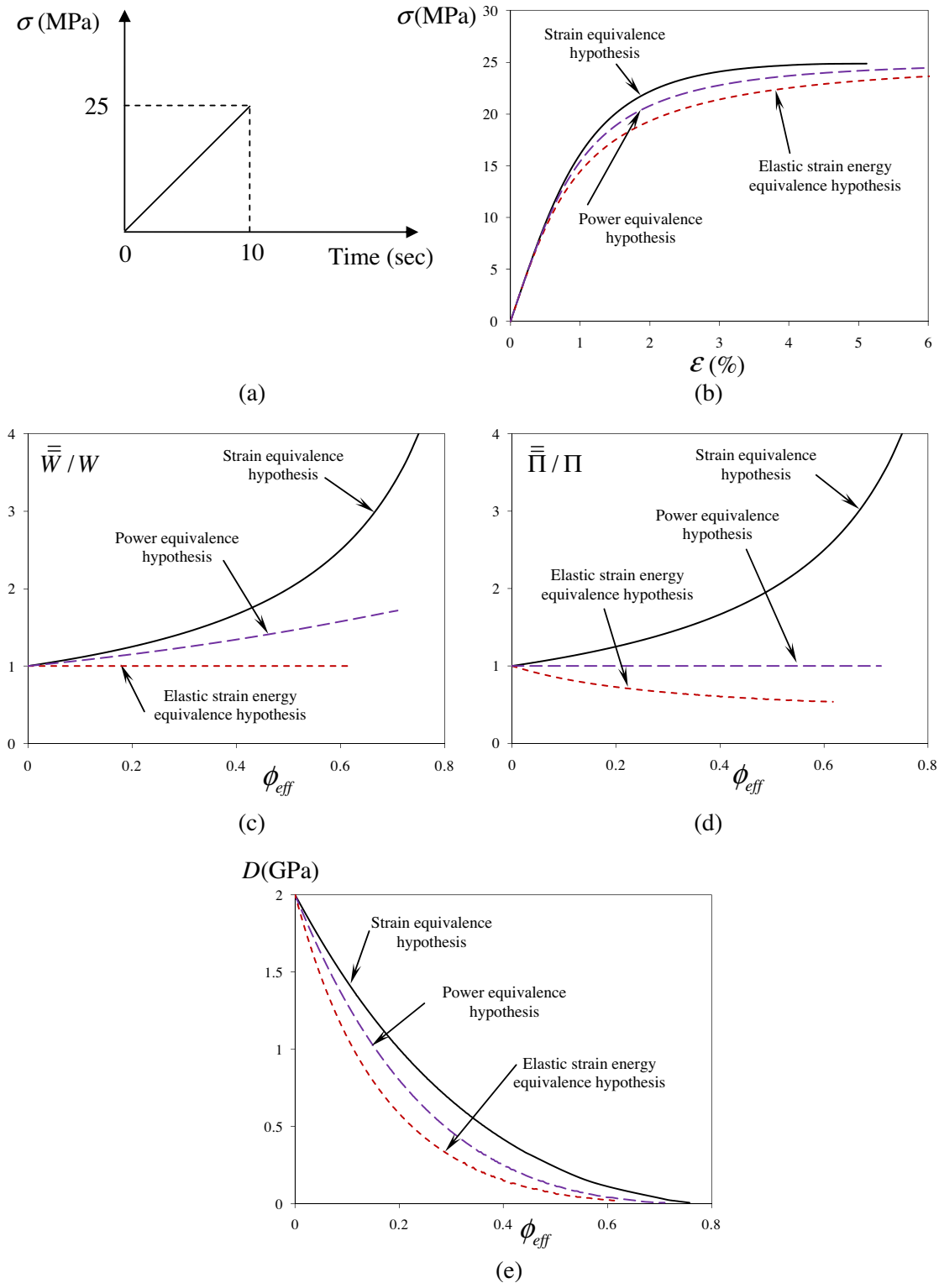

Fig. 8. Model predictions for a uniaxial constant stress rate test using different transformation hypothesis. (a) Loading history; (b) stress–strain responses; (c) ratio of the elastic strain energy in the healing configuration over that in the nominal configuration; (d) ratio of the expended power in the healing configuration over that in the nominal configuration; and (e) tangent stiffness moduli.

thermodynamic framework uses the power equivalence hypothesis since it is so far the most physically-based transformation hypotheses.

Finally, the tangent stiffness moduli for different transformation hypotheses are plotted in Fig. 7(e). The negative values of the tangent stiffness modulus show that the material is in the post peak (softening) region.

The above simulation is repeated for the case of a uniaxial constant stress rate test as well (i.e. stress-controlled uniaxial test). The loading history, stress–strain response, the ratio of the elastic

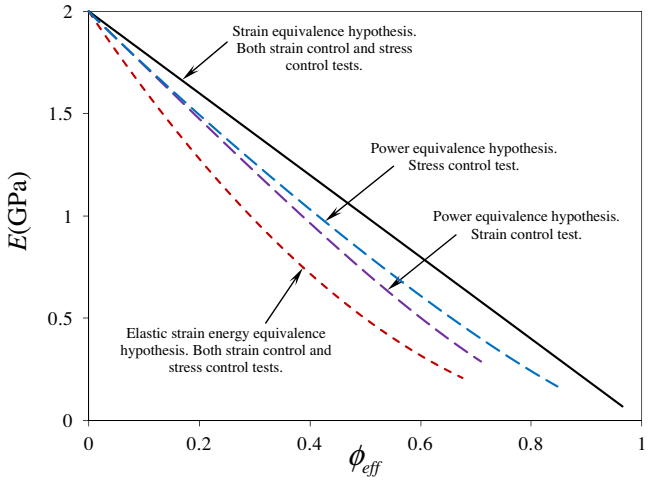

Fig. 9. Model predictions of the secant stiffness moduli for both uniaxial constant stress and uniaxial constant strain rate tests using different transformation hypotheses. The secant stiffness modulus is path-independent when strain equivalence or elastic strain energy equivalence hypotheses are used. However, secant stiffness modulus depends on loading history when the power equivalence hypothesis is used.

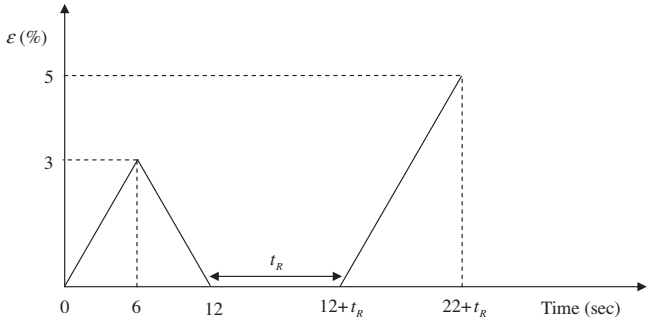

Fig. 10. Loading history for the example simulated in Section 6.2. Different rest times t_R are introduced between the loading cycles to investigate the effect of the healing level on stiffness and strength recovery.

energy in the healing and nominal configuration, the ratio of the power expenditure in the healing and nominal configurations, and the tangent stiffness using different transformation hypotheses are shown in Fig. 8(a)–(e), respectively. Comparing Figs. 7 and 8 yields similar observations for both uniaxial constant strain rate test and uniaxial constant stress rate test.

The predicted secant stiffness moduli using different transformation hypotheses are plotted in Fig. 9 for both uniaxial constant strain rate and uniaxial constant stress rate tests. Fig. 9 shows that the predicted secant moduli using the strain equivalence and elastic strain energy equivalence hypotheses are both path-independent. In other words, strain equivalence and elastic strain energy equivalence hypotheses predict unique values for the secant stiffness moduli for a specific damage density value regardless of the loading history. This behavior is expected according to Eqs. (25) and (32) for strain equivalence and elastic strain energy equivalence hypotheses, respectively. In fact, Eq. (25) shows that the secant stiffness modulus changes linearly as a function of the damage density for strain equivalence hypothesis; whereas, Eq. (32) shows that the secant stiffness modulus changes quadratic as a function of the damage density when the elastic strain energy hypothesis is postulated. On the other hand, the secant stiffness modulus becomes path-dependent when the power equivalence hypothesis is used, as shown in Fig. 9. This behavior is also expected by investigating Eq. (43). Eq. (43) clearly shows that the secant stiffness modulus is a function of the strain and strain rate in addition to the damage density value when the power equivalence hypothesis is assumed. This is a very interesting conclusion that needs to be verified experimentally, which will be the focus of a future work. Such experimental verification will be useful to decide which transformation hypothesis is more physically sound since this issue is still an open area of research. Many argue that the strain energy equivalence hypothesis is more physically sound than the strain equivalence hypothesis (e.g. Lemaître and Chaboche, 1990; Voyiadjis and Kattan, 1999; Abu Al-Rub and Voyiadjis, 2003). In fact, the current comparison shows that the power equivalence hypothesis is more physically attractive since it takes into consideration the loading path-dependency of damage evolution.

The above examples show how assuming different transformation hypotheses affect the numerical results. Therefore, each of these transformation hypotheses can be selected according to the importance of the specific quantities for a specific material. For example, the strain equivalence hypothesis can be used for simplicity when the damage density is not expected to have a significant value. The elastic energy equivalence hypothesis can be used for the elastic-damage materials where the elastic strain energy could be the driving force for the damage evolution. Finally, one may use the power equivalence hypothesis for constitutive models with the dissipative nature (such as viscoelasticity and viscoplasticity) where the elastic strain energy is negligible comparing to the total strain energy and also the dissipative power and energy becomes of great interest.

6.2. Effect of healing on stiffness recovery

In this subsection, the effect of the healing on the mechanical response of the elastic-damage-healing materials is investigated. The power equivalence hypothesis is used in this example since it is, so far, the most physically-based hypothesis. However, adapting the other transformation hypotheses will not affect the qualitative results obtained in this subsection. The rate-dependent damage and healing models are used (Eqs. (49) and (51)). The model parameters used in this section are listed in Table 1. The loading history shown in Fig. 10 can be summarized as follows:

- The material is loaded with a constant strain rate until it is partially damaged (up to 3% strain in this case).
- The load is removed with the same rate until the strain reaches zero.
- Material remains in rest for time t_R such that the induced microdamages can partially heal. As explained before, Eq. (51) is time-dependent. Hence, more damages will heal for longer rest periods. Therefore different rest periods t_R are examined to investigate the effect of different healing levels on the stiffness recovery during the reloading.
- Material is reloaded with the same strain rate until significant amount of damage is developed.

Four different rest periods of 0, 50, 200, and 500 sec are assumed in this example. Fig. 11(a) and (b) show the stress–time and stress–strain responses for different rest periods t_R, respectively. As shown in Fig. 11(a) and (b), the material recovers part of its strength and also restores its ability to carry more stress during the reloading as the rest period increases (or equivalently as the healing variable increases). Moreover, the mechanical response during the reloading becomes closer to the response of the monotonic loading as the rest period increases. A normalized rest time $\xi = t/t_R$ is defined to make the comparison of the effective damage density, ϕ_{eff}, and healing, h, variables for different rest periods easier. Hence, $\xi = 0$ indicates the start of the rest period, whereas $\xi = 1$

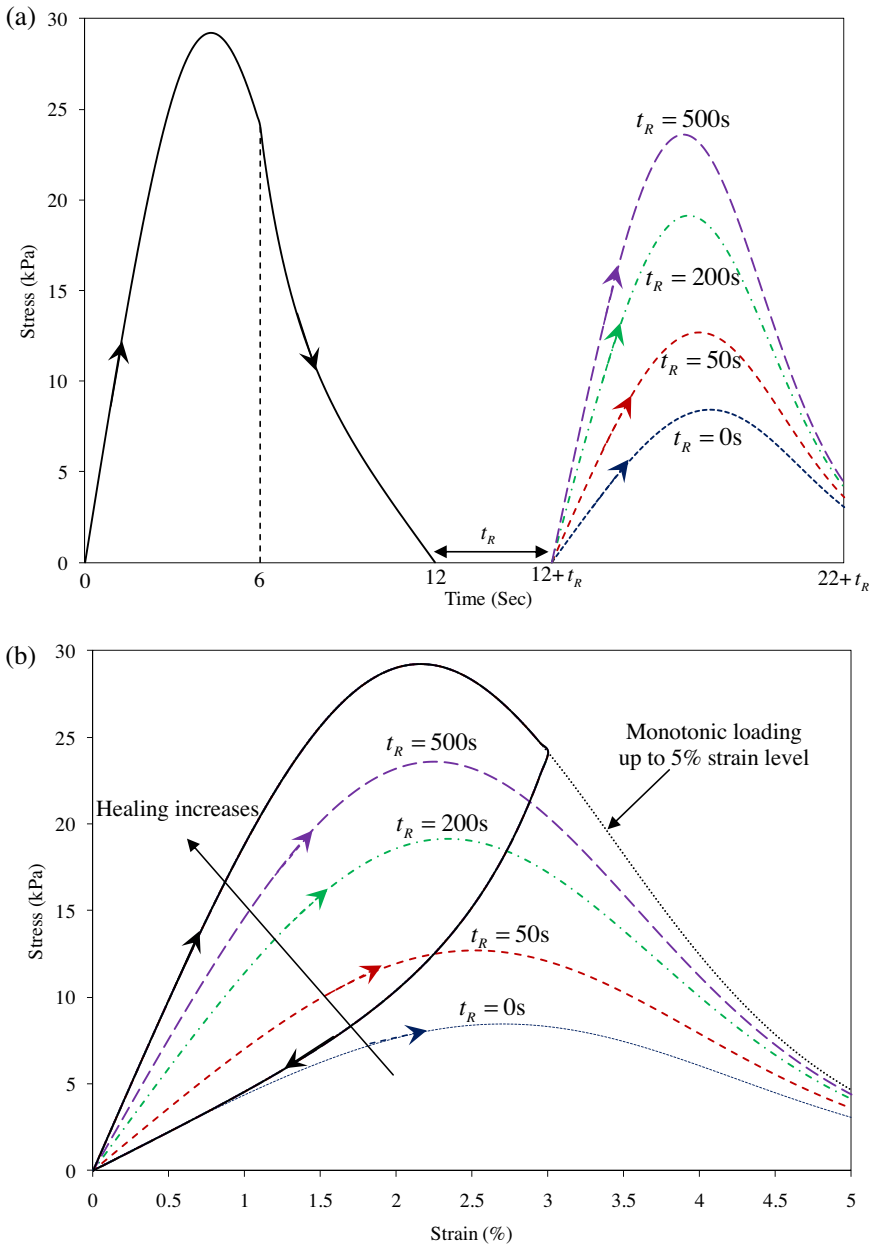

Fig. 11. (a) Stress–time; (b) stress–strain diagrams for the loading history shown in Fig. 7. Model predictions show more recovery in the stiffness during the reloading as t_R and consequently the healing variable increases.

indicates the end of the rest period. The effective damage density and healing variables are plotted versus the normalized rest time ξ in Fig. 12(a) and (b), respectively. Fig. 12(a) shows that at the beginning of the rest period the effective damage density is the same for all cases. However, the effective damage density variable decreases during the rest period as a result of micro-damage healing. Fig. 12(a) shows that the longer the rest period, the lower the effective damage density at the end of rest period. One would expect the effective damage density to reach zero and the healing variable to reach one if long enough rest period is introduced between the loading cycles. In other words, the model shows that for ideal cases, the material can retrieve all its strength and stiffness and as a result becomes identical to the virgin state of the material if put in rest for a long enough time. This can also be explained by looking at Fig. 11(b) showing that for long rest periods the material response during the reloading converges to the response of the monotonic loading.

6.3. Effect of the healing and damage models on predicting the fatigue damage

Other features of the healing model as well as the consequences of postulating rate-dependent versus rate-independent damage models are investigated in this subsection. To this end, the stress response for a cyclic loading shown in Fig. 13 is investigated. It should be mentioned that the power equivalence hypothesis is used for this examples and the ones presented in the subsequent sections. The selection of a specific transformation hypothesis will not affect the qualitative results obtained in the following examples.

6.3.1. Rate-independent damage model

The damage function presented in Eq. (53), with $\gamma = 5 \times 10^{-7}$ and $k = 50$, is used for the rate-independent damage model. The stress–strain response and the damage density versus time for

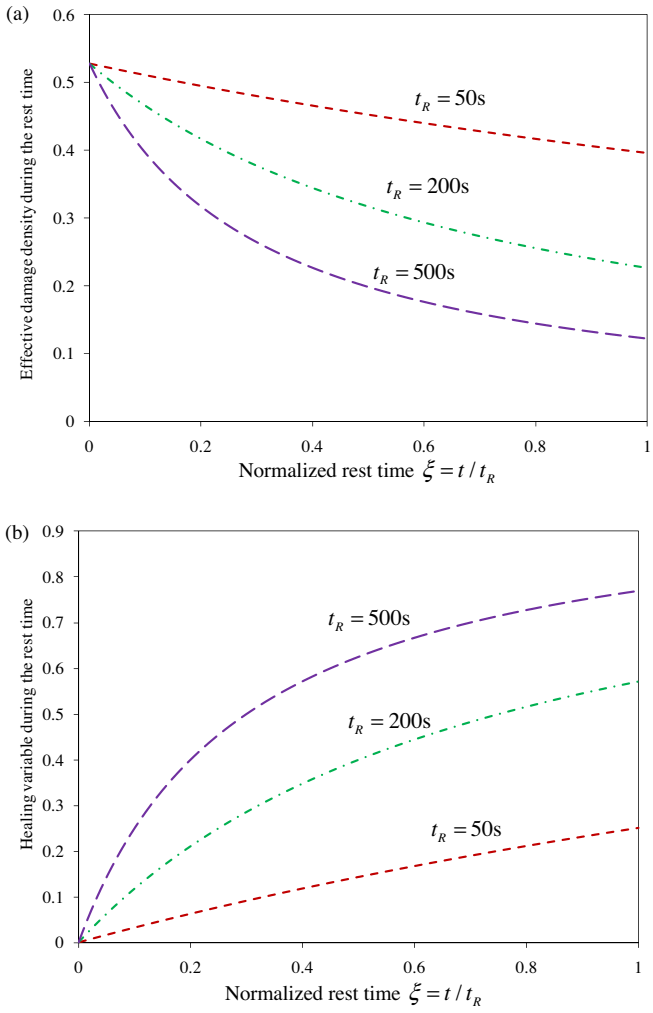

Fig. 12. (a) Effective damage density versus the normalized rest time; smaller values for the effective damage density at the end of the rest time as the rest time increases; and (b) healing variable versus the normalized rest time; more damages heal as the rest time increases.

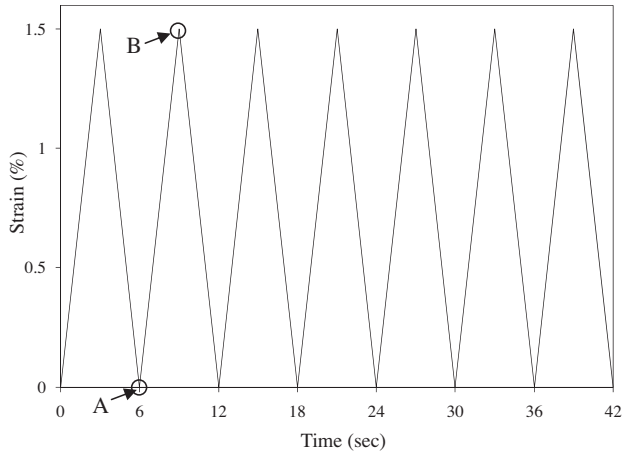

Fig. 13. The loading history for the examples presented in Section 6.3.

the elastic-damage model are shown in Fig. 14(a) and (b), respectively. As shown in Fig. 14(a), the unloading occurs linearly and no hysteresis loop occurs after the first loading cycle. In other

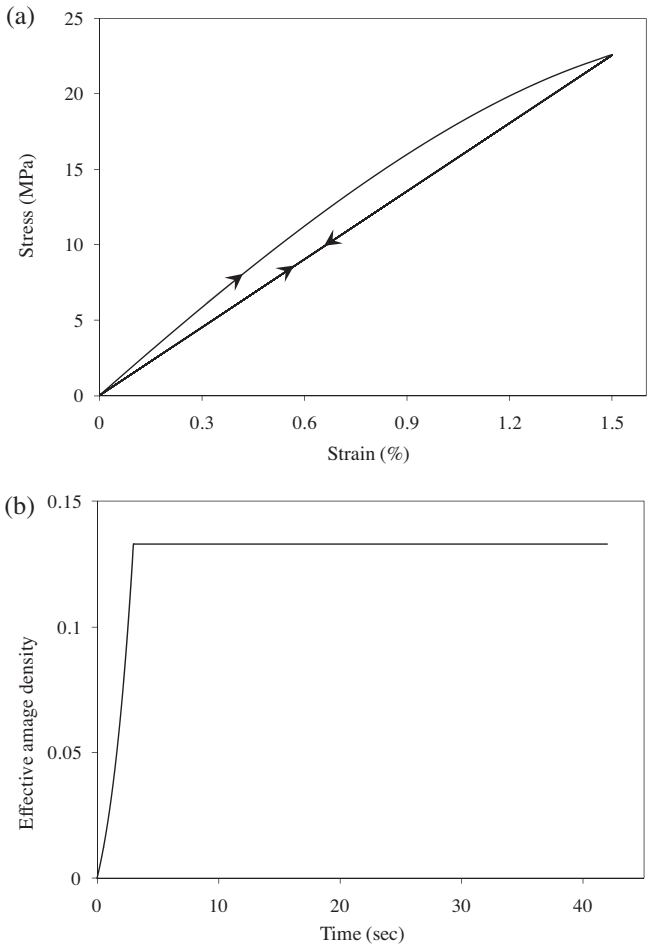

Fig. 14. Model response when using the rate-independent damage model. (a) Stress–strain response; after the first loading cycle both loading and unloading are linear. (b) Damage density versus time; damage density evolves only during the first loading cycle and remains constant during the unloading as well as during the next cycles.

words, both loading and unloading occur linearly after the first loading cycle. In this work, the damage kinematic hardening is not considered. Therefore, the damage model is a function of strain and stress level in the healing configuration which makes the damage variable to evolve only if the strain and/or stress level in the healing configuration exceed its maximum corresponding value in the first loading cycle. Obviously, the stress and strain reach its maximum value during the first loading cycle. Hence, damage does not evolve during the unloading as well as the next loading cycle which makes the presented rate-independent model incapable of predicting the nonlinear response during the unloading.

6.3.2. Rate-dependent damage model

The rate-dependent damage evolution function presented in Eq. (49) and the model parameters listed in Table 1 are used in this subsection. However, healing is not considered in this example. Assuming the rate-dependent damage model allows the damage density to evolve during both loading and unloading. In other words, damage density evolves as long as the damage driving force $\overline{\overline{Y}}$ is greater than the threshold damage force Y_{th}. However, damage evolves with slower rate during the unloading. The stress–strain response and evolution of the effective damage density (i.e. $\phi_{eff} = \phi\ (1 - h)$ where $h = 0$ since healing is not incorporated) are shown in Fig. 15(a) and (b), respectively. Fig. 15(a) shows that the model gives a nonlinear response during the unloading as well

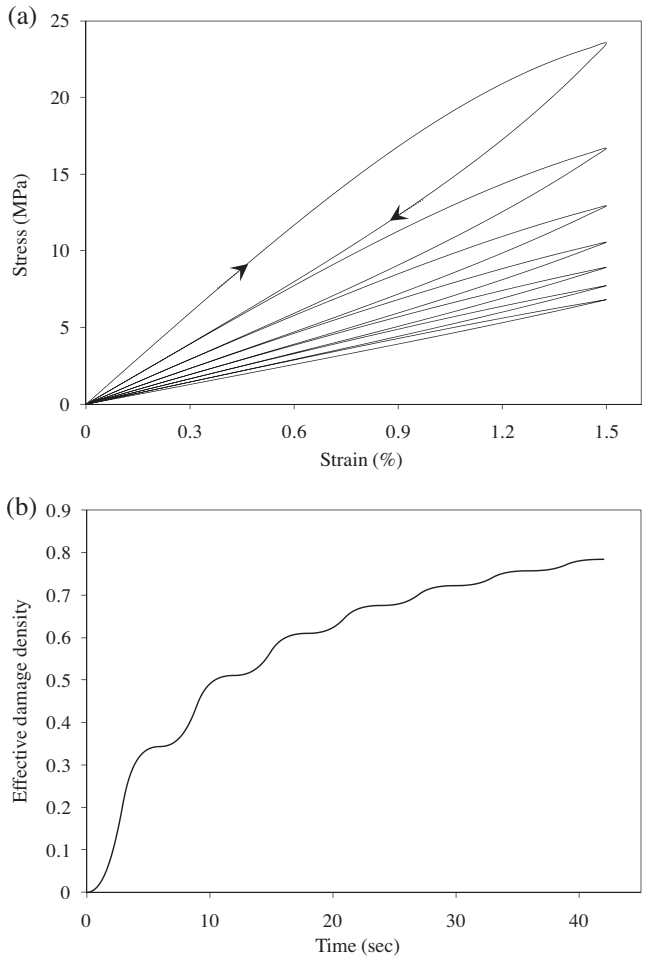

Fig. 15. Model responses for the rate-dependent damage model when healing is not considered. (a) Stress–strain response; model predicts nonlinear response during the unloading and loading, hysteresis loops form and energy dissipates at each cycle; (b) effective damage density versus time; damage density evolves during both loading and unloading at each cycle; however, the rate of damage evolution decreases as the number of loading cycles increases.

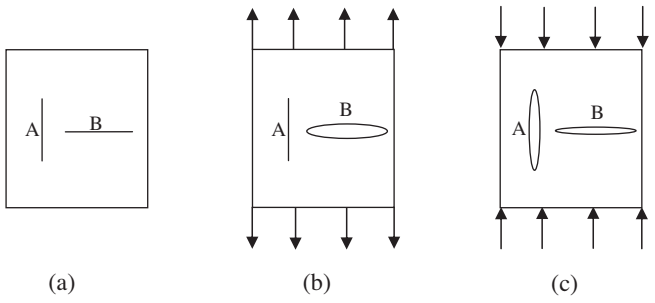

Fig. 16. Illustration of the anisotropic damage which has been postulated by Ortiz (1985) to model the nonlinear stress–strain response during the unloading. (a) A schematic RVE with two embedded cracks "A" and "B"; (b) during the loading crack "B" opens and contributes to the degradation of the stiffness; and (c) during the unloading crack "A" opens while partial crack closure occurs at crack "B". However, the net effect causes the stiffness modulus to degrade during the unloading.

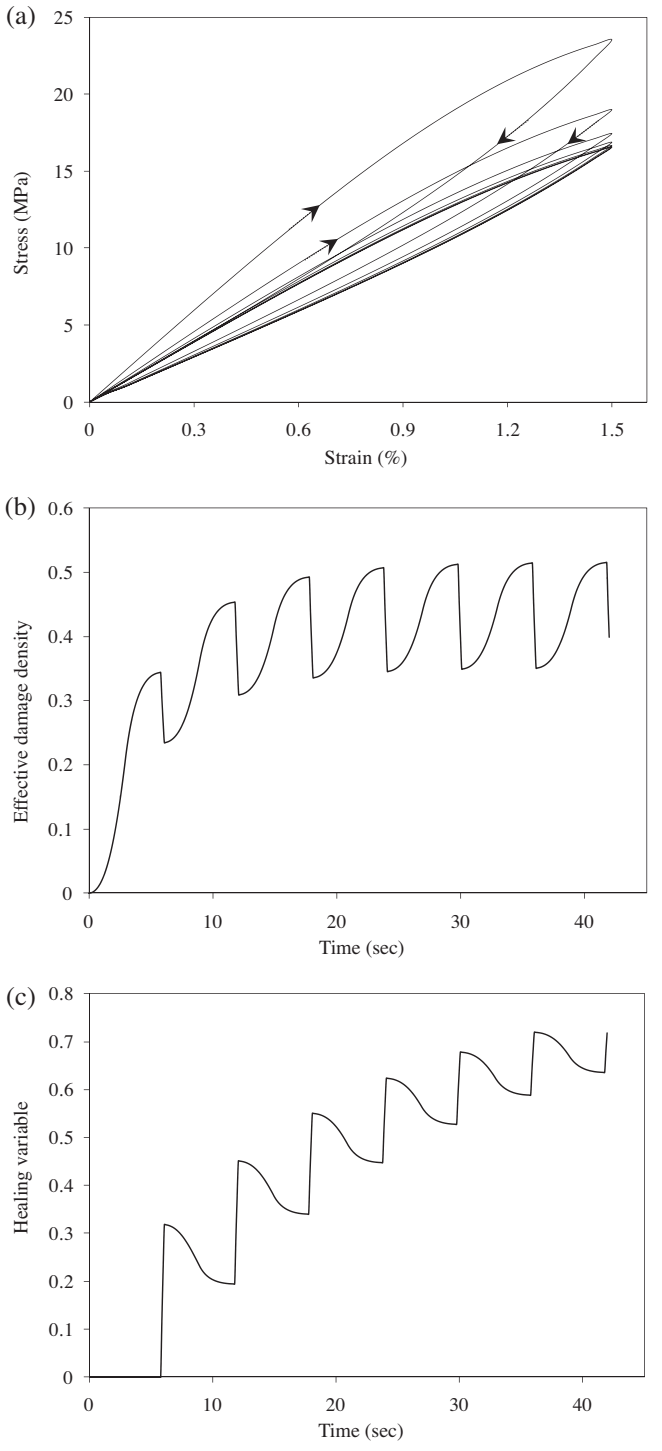

Fig. 17. Model response for the rate-dependent damage and healing models. (a) Stress–strain response; the hysteresis loops tend to converge to a single one as the number of loading cycles increases and model predictions also show the jump in the tangent stiffness modulus at unloading–loading point. (b) Effective damage density versus time; the effective damage density decreases during the unloading as a result of healing and reaches a plateau at large number of loading cycles. (c) Healing variable versus time; healing variable increases at small strain levels (close to unloading–loading points), and healing variable decreases during the loading since the total damaged area increases.

as during the loading. This is attributed to the fact that the damage density can also evolve during the unloading, as shown in Fig. 15(b).

It should be noted that Ortiz (1985) was the first to model the nonlinear response of the stress–strain diagram during unloading by considering the anisotropic damage and crack closure effects. The fundamental assumptions underlying his pioneering work are schematically illustrated in Fig. 16. Fig. 16(a) shows a schematic RVE with two embedded cracks "A" and "B" in vertical and

horizontal directions, respectively. The RVE presented in Fig. 16(a) is subjected to a uniaxial loading–unloading history. During the loading phase (Fig. 16(b)), crack "B" opens and starts growing which subsequently causes the stiffness modulus of the material to degrade. However, while crack "B" starts closing and reduces in size during the unloading phase (Fig. 16(c)), crack "A" opens and starts growing as shown in Fig. 16(c). The reduction in size of crack "B" contributes to the partial recovery in the stiffness modulus, whereas, the opening of crack "A" during the unloading contributes to the degradation of the stiffness modulus. Therefore, the change in the stiffness modulus during the unloading is a competing mechanism between the effect of the crack closure and crack opening on the stiffness during the unloading. According to the experimental observations, the tangent stiffness modulus usually decreases gradually during the unloading which is an indication of greater contribution of the crack opening during the unloading (e.g. Sinha et al., 1964; Karsan and Jirsa, 1969; Ortiz, 1985; Hassan et al., 1992; Eggeler et al., 2004; Sima et al., 2008). In this work, the anisotropic damage is not considered. However, the nonlinear response during the unloading is modeled by allowing a time-dependent degradation during the unloading through a delay-damage (i.e. viscodamage) evolution law. The net contribution of the closure of crack "A" and opening of crack "B" (Fig. 16) on the stiffness reduction during the unloading is captured by allowing the material to gradually feel the presence of existing cracks during the unloading through crack closure/opening processes. In other words, at the onset of unloading the material memorizes the damaged stiffness from the previous loading cycle such that the presence of the newly developed micro-cracks during the current loading cycle is not felt yet by the material. However, upon more unloading a gradual opening/closure of existing cracks occurs so that the material starts gradually feel the presence of those newly developed cracks that will subsequently cause a gradual stiffness reduction until the complete unloading as schematically shown in Fig. 1.

Consequently, one may argue that the commonly observed nonlinear response in the stress–strain diagram during the unloading could be due to more damage accumulation. However, careful and extensive experimental measurements should be conducted before one may prove this argument for a specific type of material. Moreover, Fig. 15(a) shows that when damage is allowed to evolve during the unloading, hysteresis loops form for each loading–unloading cycle. Hence, energy dissipation continues even after the first loading–unloading cycle which could trigger the fatigue damage.

The experimental investigations on the cyclic loading of several materials also show a jump in the tangent stiffness modulus at the unloading–loading points (e.g. point "A" in the loading history presented in Fig. 13) (e.g. Sinha et al., 1964; Karsan and Jirsa, 1969; Ortiz, 1985; Hassan et al., 1992). In other words, the tangent stiffness at the end of the unloading is usually less than the tangent stiffness at the beginning of the next reloading. However, the rate-dependent damage model is not able to predict this phenomenon as shown in Fig. 15(a).

6.3.3. Rate-dependent damage and healing models

Rate-dependent damage and healing models presented respectively in Eqs. (49) and (51) are considered in this section. The damage model parameters are as listed in Table 1. However, the healing model parameters are modified to expedite the healing evolution $\left(\Gamma^h = 0.8\ \mathrm{s}^{-1},\ m = 1,\ \bar{\varepsilon}^h_{th} = 0.001\right)$ in order to magnify the healing effect. The stress–strain response, evolution of the effective damage density (i.e. $\phi_{eff} = \phi(1-h)$), and the evolution of the healing variable are shown in Fig. 17(a)–(c), respectively. Fig. 17(a) shows the model's ability to predict nonlinear responses during the unloading. It also shows the formation of hysteresis loops for each loading cycles. However, interestingly, the model shows the jump in the tangent stiffness at unloading–loading point (e.g. point "A" in Fig. 13) when healing is included (this jump can be seen more clearly in Fig. 11(b) where the tangent stiffness at the end of unloading is less than that at the beginning of the reloading when healing is considered). Moreover, the hysteresis loops converge to a single loop at high loading cycles and tend to stabilize as shown in Fig. 17(a) (Fig. 17(a) shows that the hysteresis loop for loading cycles 5–7 are very close together and tend to converge to a single loop). As mentioned before, the healing condition presented in Eq. (52) indicates that the healing variable starts evolving once the total effective strain is less than the threshold healing strain. Hence, in the regions close to unloading–loading point (e.g. point "A" in Fig. 13) where strain is close to zero, the healing variable increases and subsequently the effective damage density decreases. Therefore, the material recovers part of its strength and stiffness at unloading–loading point that causes the stiffness to show a jump at this point. This observation can also be explained by looking at the effective damage density variable. As shown in Fig. 17(b), the effective damage density reaches a plateau as the number of loading cycle increases. In other words, the newly nucleated micro-damages at large number of loading cycle heals at unloading–loading point, and hence, the effective damage density reaches a plateau where no more damage accumulation occurs during the next loading cycle. It also shows that, unlike the commonly postulated assumptions in CDM, the effective damage density is reversible as a result of micro-damage healing. Therefore, one may argue that the jump in stiffness at unloading–loading points might be due to micro-damage healing at low strain levels. Again, careful experimental tests should be conducted to prove this argument. Fig. 17(c) shows that the healing variable decreases during the loading. This decrease can be explained according to Eq. (61). During loading, the area of unhealed damages A^{uh} increases. Therefore, although the area of the healed damages A^h does not change during the loading, the healing variable decreases since it is defined as the ratio of the healed damages' area over the total damaged area (i.e. $h = A^h/A^D$).

7. Conclusions

A novel continuum damage mechanics-based framework is proposed in this paper to enhance the continuum damage mechanics theories in modeling the micro-damage healing phenomenon in materials that tend to self-heal. This framework is proposed by extending the concept of the effective configuration and effective stress to the healing configuration.

Three well-known transformation hypotheses of the continuum damage mechanics theories (i.e. strain, elastic strain energy, and power equivalence hypotheses) are also extended for the materials with healing ability. Analytical relations are derived for each transformation hypothesis to relate the strain tensors, secant stiffness moduli, and tangent stiffness moduli in the damaged (nominal) and healing configurations.

The presented examples demonstrate that the proposed healing framework captures the recovery in strength and stiffness modulus when healing occurs. These examples of the effect of rest periods between loading cycles show that the model predicts increased levels of recovery in the stiffness and strength as the resting period increases.

It is argued that the commonly observed nonlinear responses during the unloading in the stress–strain response can be modeled using the rate- and time-dependent damage models. Therefore, it is implied that these nonlinear responses could be because of the delay-damage response (viscodamage) during the unloading.

It is also shown that the jump in the tangent stiffness modulus at unloading–loading points might be related to micro-damage healing at very small strains.

Acknowledgements

Authors acknowledge the financial support provided by the Federal Highway Administration. Also, financial support by the Qatar National Research Fund (Award 08-310-2-110) is acknowledged.

Appendix A. Thermodynamic framework for constitutive modeling of the damage and micro-damage healing

This Appendix presents a general thermodynamic framework for constitutive modeling of damage and micro-damage healing mechanisms. The damage and micro-damage healing models of Darabi et al. (2011a) and Abu Al-Rub et al. (2010) are also derived systematically based on the presented thermodynamic framework. It should be noted that slight modifications are required to generalize this framework to self-healing materials with chemical reactivity (such as the hydration reactions or pozzolanic reactions during the curing of Portland cement).

This framework is used to derive an elastic-damage-healing constitutive model. It should be noted that the experimental observations show that specific materials such as bituminous materials undergo healing process during rest periods (i.e. the external loading is removed from the body). Also, several studies have shown that temperature has a significant effect on healing rate (e.g. Reinhardt and Jooss, 2003; Kessler, 2007; Little and Bhasin, 2007). In other words, temperature speeds up the healing process and in some cases is essential for complete healing. In these cases, the introduction of heat required for the healing process cannot be ignored (e.g. Cardona et al., 1999).

One can start with the principle of virtual power which states that the external expenditure of the power P_{ext} due to a virtual motion should be balanced by the internal expenditure of the power P_{int} associated with the same virtual motion, such that:

$$P_{\text{int}} = P_{\text{ext}} \tag{A1}$$

Degrees of freedom of the body are considered to be the displacement vector $\boldsymbol{u}$, the elastic strain tensor $\boldsymbol{\varepsilon}^e$, the damage density ϕ, the healing variable h, and the temperature T; such that the generalized virtual motions is the set consisting of $\{\dot{\boldsymbol{u}}, \dot{\boldsymbol{\varepsilon}}^e, \dot{\phi}, \dot{\boldsymbol{h}}, \dot{\boldsymbol{T}}, \nabla\dot{T}\}$. It is assumed that these virtual motions are, momentarily, independent. However, the dependency among these virtual motions will be established later. It should be noted that the rate of temperature $\dot{T}$ and its gradient $\nabla\dot{T}$ have been added to the usual velocity variables to ensure the generality of the thermodynamic framework and in consideration of the endothermic nature of the healing process. Obviously, conventional energy flux should also be modified according to Maugin and Muschik (1994). The internal expenditure of virtual power can be written as follows:

$$P_{\text{int}} = \int_V (\boldsymbol{\sigma} : \dot{\boldsymbol{\varepsilon}}^e + Y\dot{\phi} - H\dot{h} + \xi\dot{T} + \boldsymbol{\gamma}.\nabla\dot{T})dV \tag{A2}$$

The Cauchy stress tensor $\boldsymbol{\sigma}$, the damage force Y, and the healing force H are the generalized thermodynamic forces conjugate to the elastic strain tensor, damage density, and healing variable, respectively. Two additional generalized thermodynamic forces ξ and $\boldsymbol{\gamma}$ conjugate to temperature and its gradient, respectively, are defined similar to Cardona et al. (1999).

It should be noted that Eq. (A2) shows that the damage process increases the internal expenditure of power, whereas, the micro-damage healing process decreases the internal expenditure of power. This micro-damage healing process can therefore be considered as the inverse of the damage process.

On the other hand, the macroscopic body force $\boldsymbol{b}$, the macroscopic surface traction $\boldsymbol{t}$, the inertial forces, and the generalized temperature traction χ conjugate to $\dot{T}$ contribute to the external expenditure of power, such that:

$$P_{\text{ext}} = \int_V b_i\dot{u}_i dV + \int_S t_i\dot{u}_i dS - \int_V \rho\ddot{u}_i\dot{u}_i dV + \int_S \chi\dot{T}dS \tag{A3}$$

Based on the principle of virtual power (Eq. (A1)) and with some mathematical manipulations, one obtains:

$$\sigma_{ij,j} + b_i = \rho\ddot{u}_i; \quad \text{in } V \tag{A4}$$

$$t_i = \sigma_{ij}n_j; \quad \text{on } S \tag{A5}$$

$$\chi = \gamma_i n_i; \quad \text{on } S \tag{A6}$$

$$Y = 0; \quad \text{in } V \tag{A7}$$

$$-H\dot{h} + (\xi - \gamma_{i,i})\dot{T} = 0; \quad \text{in } V \tag{A8}$$

where $\boldsymbol{n}$ denotes the outward unit normal on the boundary $\boldsymbol{S}$. Eqs. (A4) and (A5) represent the local static/dynamic macroforce balance and the boundary traction as the density of the surface forces, respectively. Eq. (A6) defines the boundary traction for the thermodynamic forces conjugate to $\dot{T}$. Eq. (A7) defines the damage microforce balance (Fremond and Nedjar, 1996) which will be used to derive the dynamic viscodamage nucleation and growth conditions. The virtual motion fields have not been removed in Eq. (A8). This new and non-classical equation will be referred to as the *micro-damage healing microforce balance* which will be used to derive micro-damage healing condition and evolution functions. To the authors' best knowledge, this microforce balance to describe micro-damage healing has not be derived before. Eq. (A8) reduces to the following equation when the gradient of the rate of temperature is neglected (i.e. $\nabla\dot{T} \cong 0$):

$$-H\dot{h} + \xi\dot{T} = 0 \tag{A9}$$

Eq. (A9) clearly shows the dependency of the healing process on the rate of temperature. Roughly speaking, Eq. (A9) states that additional power provided as external heat is required for the healing process to occur. This is in agreement with the endothermic nature of the healing process. This equation can be explained even for the isothermal conditions for which the body V is in contact with a reservoir maintaining a constant temperature. In other words, in this case, the healing process is accompanied by the absorption of the heat from its surrounding area. This process causes the temperature drop within the area in which healing occurs. The reservoir will then compensate for this temperature drop by supplying the heat to the body V guaranteeing the isothermal condition. However, the time scale for achieving the isothermal condition is of the order of the time scale required for the healing phenomenon which makes it impossible, for practical purposes, to ignore this transient region during the healing process. Again, the rate of the heat supply is directly correlated to the rate of the healing process. Therefore, as the first approximation, one can assume a linear relationship between the rate of the temperature change and the healing rate (i.e. $\xi\dot{T} = K\dot{h}$), such that the micro-damage healing microforce balance will be simplified to the following form in the absence of the temperature gradient:

$$H - K = 0 \tag{A10}$$

As previously mentioned, the healing configuration is defined as a fictitious state where the unhealed damage areas are removed from the material. Hence, unhealed damage does not contribute to the internal expenditure of power in the healing configuration. Therefore, one can simply express the internal expenditure of power in the healing configuration, $\overline{\overline{P}}_{\text{int}}$, as follows:

$$\overline{\overline{P}}_{\text{int}} = \int_V \bar{\boldsymbol{\sigma}} : \delta\dot{\bar{\boldsymbol{\varepsilon}}}^e dV \tag{A11}$$

However, as it was shown in Eqs. (A7) and (A10), the damage and micro-damage healing balance laws are always null (i.e. $Y = 0$ and

$H - K = 0$). Hence, by using the power equivalence hypothesis and Eqs. (A7) and (A10), it can be shown that Eqs. (A2) and (A11) are the same, such that:

$$\bar{\bar{P}}_{\text{int}} = P_{\text{int}} \tag{A12}$$

Moreover, it is assumed that, for the isothermal conditions, the Helmholtz free energy Ψ depends on the elastic strain tensor $\bar{\bar{\varepsilon}}^e$, the damage density ϕ, and the healing variable h, such that:

$$\Psi = \Psi(\bar{\bar{\varepsilon}}^e, \phi, h) \tag{A13}$$

By combining the first and second laws of thermodynamics (i.e. balance of energy and entropy imbalance, respectively), conservation of mass, the Clausius–Duhem inequality can be written as follows for the isothermal conditions (c.f. Lemaître and Chaboche, 1990):

$$\int_V \rho \dot{\Psi} dV \leqslant P_{\text{int}} \tag{A14}$$

Taking the time derivative of Eq. (A13) and substitute into Eq. (A14) yield:

$$\left(\bar{\bar{\sigma}} - \rho \frac{\partial \Psi}{\partial \bar{\bar{\varepsilon}}^e}\right) : \dot{\bar{\bar{\varepsilon}}}^e + \left(Y - \rho \frac{\partial \Psi}{\partial \phi}\right)\dot{\phi} - \left(H + \rho \frac{\partial \Psi}{\partial h}\right)\dot{h} + K\dot{h} \geqslant 0 \tag{A15}$$

from which the following classical thermodynamic state law for the Cauchy stress as the thermodynamic conjugate force of the elastic strain tensor is defined:

$$\bar{\bar{\sigma}} = \rho \frac{\partial \Psi}{\partial \bar{\bar{\varepsilon}}^e} \tag{A16}$$

such that the rate of the energy dissipation Π can be written as:

$$\Pi = \left(Y - \rho \frac{\partial \Psi}{\partial \phi}\right)\dot{\phi} - \left(H + \rho \frac{\partial \Psi}{\partial h}\right)\dot{h} + K\dot{h} \geqslant 0 \tag{A17}$$

As previously mentioned, a specific location within the material at a specific time t can either undergo the damage process or undergo the micro-damage healing process. Therefore, the rate of the micro-damage healing variable is zero during the damage process and vice versa. The rate of the energy dissipation during the damage process Π^{vd} and during the micro-damage healing process Π^h can be expressed as follows:

$$\Pi^{vd} = \left(Y - \rho \frac{\partial \Psi}{\partial \phi}\right)\dot{\phi} \tag{A18}$$

$$\Pi^h = -\left(H + \rho \frac{\partial \Psi}{\partial h}\right)\dot{h} + K\dot{h} \tag{A19}$$

such that the total rate of energy dissipation can be written as:

$$\Pi = \Pi^{vd} + \Pi^h \geqslant 0 \tag{A20}$$

It should be noted that during the damage process the rate of the micro-damage healing variable vanishes (i.e. $\dot{h} = 0$). Therefore, during the damage process, Π represents the rate of the energy dissipation due to damage nucleation and growth such that one can write:

$$\Pi = \Pi^{vd} = \left(Y - \rho \frac{\partial \Psi}{\partial \phi}\right)\dot{\phi} \geqslant 0; \;\; \dot{h} = 0 \,(\text{during the damage}) \tag{A21}$$

Eq. (A21) shows that the value of the expended internal power due to the damage process is greater than the energy stored inside the material due to damage hardening. Therefore, part of the expended power due to the damage process should have been dissipated (i.e. Π^{vd}).

Similarly, during the micro-damage healing process the rate of the damage variable is zero (i.e. $\dot{\phi} = 0$). In this case, Π represents the rate of the energy dissipation due to the micro-damage healing process such that one can write:

$$\Pi = \Pi^h = -\left(H + \rho \frac{\partial \Psi}{\partial h}\right)\dot{h} + K\dot{h} \geqslant 0;$$

$$\dot{\phi} = 0 \,(\text{during the micro-damage healing}) \tag{A22}$$

A close look at Eq. (A22) shows that part of the required internal power for the micro-damage healing process is provided by the stored energy due to the micro-damage healing processes. In other words, the micro-damage healing process causes the stored energy to decrease. This released energy (provided by the decrease in the stored energy) is derived from the surface free energy on the faces of the cracks that participate in the healing process as well as from, in certain systems, the increase in configurational entropy. For example, in a bitumen system, the introduction of a crack face probably establishes a preferred orientation of aliphatic, polynuclear aromatic and naphtenic aromatics. During the healing process a reorganization of these phase or components across the crack interface contributes to some degree to the re-establishment of strength, healing, resulting in an increase in configurational entropy and a decrease in free energy. In fact, Bhasin et al. (2011) established, using molecular dynamics, that the composition of the bitumen affects the rate or reorganization across an interface. This released energy is spent for partial micro-damage healing process. The extra required energy for the micro-damage healing process (i.e. shown by $K\dot{h}$) comes from the external heat energy (i.e. $\xi\dot{T} = K\dot{h}$). For the hypothetical completely self-healing materials this extra energy is not required (i.e. $K = 0$), such that the micro-damage healing process does not dissipate energy and can be considered as a reversible process. However, this condition does not occur in reality.

Eqs. (A21) and (A22) contain terms which are only a function of the Helmholtz free energy, such that one can define those as the energetic terms as follows:

$$Y^{\text{ene}} \equiv \rho \frac{\partial \Psi}{\partial \phi} \tag{A23}$$

$$H^{\text{ene}} \equiv -\rho \frac{\partial \Psi}{\partial h} \tag{A24}$$

where Y^{ene} and H^{ene} are energetic components of the thermodynamic forces conjugate to ϕ and h, respectively, which contribute to the decrease or the increase in the Helmholtz free energy. Substituting Eqs. (A23) and (A24) respectively into Eqs. (A21) and (A22) yields:

$$\Pi = (Y - Y^{\text{ene}})\dot{\phi} - (H - H^{\text{ene}})\dot{h} + K\dot{h} \geqslant 0 \tag{A25}$$

Eq. (A25) shows that the rate of the energy dissipation resulting from damage process is positive only if the thermodynamic force conjugate to damage variable has both energetic and dissipative components, such that the rate of the energy dissipation due to damage process can be written as:

$$\Pi = \Pi^{vd} = Y^{\text{dis}}\dot{\phi} \geqslant 0; \;\; \dot{h} = 0 \,(\text{during the damage process}) \tag{A26}$$

Similarly, one can define a dissipative micro-damage healing conjugate force, such that during the healing process the rate of the energy dissipation can be written as follows:

$$\Pi = \Pi^h = (-H^{\text{dis}} + K)\dot{h} \geqslant 0;$$

$$\dot{\phi} = 0 \,(\text{duringthe micro-damage healing process}) \tag{A27}$$

where Y^{dis} and H^{dis} are dissipative components of the damage and micro-damage healing conjugate forces, respectively, and are defined as follows:

$$Y^{\text{dis}} = Y - Y^{\text{ene}} \tag{A28}$$

$$H^{\text{dis}} = H - H^{\text{ene}} \tag{A29}$$

The presented thermodynamic framework shows that both damage and micro-damage healing thermodynamic forces should have energetic and dissipative components. This is in line with

the pioneering work of Ziegler (1977) which states that the proper estimation of the stored energy and energy dissipation requires the thermodynamic conjugate forces to have both energetic and dissipative components. It should be noted that Alfredsson and Stigh (2004) and Barbero et al. (2005) also proposed thermodynamic-based micro-damage healing models. However, they did not decompose the damage and micro-damage healing forces into energetic and dissipative components. The energetic and dissipative terms mean that the thermodynamic conjugate forces are derived from the Helmholtz free energy and the rate of the energy dissipation, respectively. Obviously, in order to formulate constitutive equations for the energetic and dissipative conjugate forces, one needs to know how the material stores energy (which helps in assuming a mathematical form for the Helmholtz free energy) and how the material dissipates energy (which helps in assuming mathematical forms for the rate of the energy dissipation).

The dissipative components of the thermodynamic conjugate forces can be identified using the maximum rate of energy dissipation principle and utilizing the mathematics of multiple variables, such that:

$$Y^{\text{dis}} = \lambda^{vd}\frac{\partial \Pi}{\partial \dot{\phi}} \tag{A30}$$

$$H^{\text{dis}} - K = -\lambda^{h}\frac{\partial \Pi}{\partial \dot{h}} \tag{A31}$$

where λ^{vd} and λ^{h} are viscodamage and micro-damage healing Lagrange multipliers, respectively, which can be identified using the calculus of multiple variables, such that:

$$\lambda^{vd} = \Pi \Big/ \left(\frac{\partial \Pi}{\partial \dot{\phi}}\dot{\phi}\right); \quad \lambda^{h} = \Pi \Big/ \left(\frac{\partial \Pi}{\partial \dot{h}}\dot{h}\right) \tag{A32}$$

The next step is to assume mathematical forms for the Helmholtz free energy and the rate of the energy dissipation function. In this work, the following forms are assumed for the Helmholtz free energy and rate of the energy dissipation, respectively, in order to derive the damage model of Darabi et al. (2011a) and the micro-damage healing model of Abu Al-Rub et al. (2010):

$$\rho\Psi = \frac{1}{2}\bar{\bar{\boldsymbol{\varepsilon}}}^{e} : \bar{\bar{\boldsymbol{E}}} : \bar{\bar{\boldsymbol{\varepsilon}}}^{e} + \Gamma_1(1-\phi)(1-h) \tag{A33}$$

$$\Pi = \Gamma_2(1-\phi)^{c_1}(1-h)\left(\frac{\bar{\bar{Y}}}{Y_{th}}\right)^{c_2}\exp(c_3\bar{\bar{\boldsymbol{\varepsilon}}}_{eff})\dot{\phi}^2 + \Gamma_3(1-\phi)^{c_4}(1-h)^{c_5}\dot{h}^2 \tag{A34}$$

The second term of Eq. (A33) will be zero when $\phi = 0$ or $\phi = 1$. These cases mean that either the material has not been damaged or the induced damages have been healed. For both cases, the nominal and healing configurations are the same such that the stored energy is only due to the elastic deformation. Moreover, this equation shows that for a constant damage level, the stored energy decreases as the micro-damage healing variable increases.

The damage and micro-damage healing microforce balances are presented in Eqs. (A7) and (A10), respectively, and rewritten as follows:

$$Y = 0 \Rightarrow Y^{\text{ene}} + Y^{\text{dis}} = 0 \Rightarrow Y^{\text{ene}} = -Y^{\text{dis}} \tag{A35}$$

$$H - K = 0 \Rightarrow H^{\text{ene}} + H^{\text{dis}} - K = 0 \Rightarrow H^{\text{ene}} = -(H^{\text{dis}} - K) \tag{A36}$$

The energetic and dissipative components of the thermodynamic conjugate forces can be identified by substituting Eqs. (A33) and (A34) into Eqs. (A23), (A24), (A30), and (A31), such that:

$$Y^{\text{ene}} = -\Gamma_1(1-h); \; Y^{\text{dis}} = \Gamma_2(1-\phi)^{c_1}(1-h)\left(\frac{\bar{\bar{Y}}}{Y_{th}}\right)^{c_2}\exp(c_3\bar{\bar{\boldsymbol{\varepsilon}}}_{eff})\dot{\phi} \tag{A37}$$

$$H^{\text{ene}} = \Gamma_1(1-\phi); \; H^{dis} - K = -\Gamma_3(1-\phi)^{c_4}(1-h)^{c_5}\dot{h} \tag{A38}$$

The damage evolution function of Darabi et al. (2011a) (Eq. (45)) can now be derived by substituting Eq. (A37) into Eq. (A35), such that:

$$\dot{\phi} = \Gamma^{vd}\left(\frac{\bar{\bar{Y}}}{Y_{th}}\right)^{q}(1-\phi)^2\exp(k\bar{\bar{\boldsymbol{\varepsilon}}}_{eff}) \tag{A39}$$

where $\Gamma^{vd} = \Gamma_1/\Gamma_2$, $q = -c_2$, $c_1 = -2$, and $k = -c_3$. Similarly, the micro-damage healing evolution function of Abu Al-Rub et al. (2010) (Eq. (48)) can be determined by substituting Eq. (A38) into Eq. (A36), such that:

$$\dot{h} = \Gamma^{h}(1-\phi)^{m_1}(1-h)^{m_2} \tag{A40}$$

where $\Gamma^{h} = \Gamma_1/\Gamma_3$, $m_1 = 1 - c_4$, and $m_2 = -c_5$.

It is noteworthy that the presented thermodynamic framework for the damage and micro-damage healing processes is general and can be used to derive different constitutive models for the damage and micro-damage healing mechanisms. Coupling of the damage and micro-damage healing processes to the viscoelastic, viscoplastic, and temperature will be the subject of a future work by the current authors.

References

Abaqus, 2008. Version 6.8. Habbit, Karlsson and Sorensen, Inc, Providence, RI.

Abu Al-Rub, R.K., Voyiadjis, G.Z., 2003. On the coupling of anisotropic damage and plasticity models for ductile materials. International Journal of Solids and Structures 40, 2611–2643.

Abu Al-Rub, R.K., Darabi, M.K., Little, D.N., Masad, E.A., 2010. A micro-damage healing model that improves prediction of fatigue life in asphalt mixes. International Journal of Engineering Science 48, 966–990.

Adam, J.A., 1999. A simplified model of wound healing (with particular reference to the critical size defect). Mathematical and Computer Modelling 30, 23–32.

Alfredsson, K.S., Stigh, U., 2004. Continuum damage mechanics revised: A principle for mechanical and thermal equivalence. International Journal of Solids and Structures 41, 4025–4045.

Ando, K., Chu, M.C., Tsuji, K., Hirasawa, T., Kobayashi, Y., Sato, S., 2002. Crack healing behaviour and high-temperature strength of mullite/sic composite ceramics. Journal of the European Ceramic Society 22, 1313–1319.

Arrington, E.D., Smith, W.J., Chambers, H.G., Bucknell, A.L., Davino, N.A., 1996. Complications of iliac crest bone graft harvesting. Clinical Orthopaedics and Related Research 329, 300–309.

Barbero, E.J., Greco, F., Lonetti, P., 2005. Continuum damage-healing mechanics with application to self-healing composites. International Journal of Damage Mechanics 14, 51–81.

Bari, S., Hassan, T., 2000. Anatomy of coupled constitutive models for ratcheting simulation. International Journal of Plasticity 16, 381–409.

Bhasin, A., Little, D.N., Bommavaram, R., Vasconcelos, K., 2008. A framework to quantify the effect of healing in bituminous materials using material properties. Road Materials and Pavement Design 9, 219–242.

Bhasin, A., Bommavaram, R., Greenfield, M.L., Little, D.N., 2010. Use of molecular dynamics to investigate self-healing mechanisms in asphalt binders. Journal of Materials in Civil Engineering (ASCE). doi:10.1061/(ASCE)MT.1943-5533.0000200.

Bhasin, A., Bommavaram, R., Greenfield, M.L., Little, D.N., 2011. Use of molecular dynamics to investigate self-healing mechanisms in asphalt binders. Journal of Materials in Civil Engineering (ASCE) 23, 485–492.

Bond, I., Trask, R., Williams, G., Williams, H., 2007. Autonomic self-healing and damage visualisation in fibre reinforced polymer composites. Structural Health Monitoring: Quantification, Validation, and Implementation 1, 1364–1372.

Brown, E.N., Sottos, N.R., White, S.R., 2002. Fracture testing of a self-healing polymer composite. Experimental Mechanics 42, 372–379.

Brown, E.N., White, S.R., Sottos, N.R., 2005. Retardation and repair of fatigue cracks in a microcapsule toughened epoxy composite. Part ii: in situ self-healing. Composites Science and Technology 65, 2474–2480.

Cardona, J.-M., Forest, S., Sievert, R., 1999. Towards a theory of second grade thermoelasticity. Extracta Mathematicae 14, 127–140.

Coleman, B.D., Gurtin, M.E., 1967. Thermodynamics with internal state variables. Journal of Chemical Physics 47, 597–613.

Collins, I.F., Houlsby, G.T., 1997. Application of thermomechanical principles to the modelling of geotechnical materials. Proceedings of the Royal Society of London A 453, 1975–2001.

Cordebois, J., Sidoroff, F., 1982. Anisotropic damage in elasticity and plasticity. Journal De Mecanique Theorique Et Appliquee, 45–60.

Darabi, M.K., Abu Al-Rub, R.K., Masad, E.A., Huang, C.-W., Little, D.N., 2011a. A thermo-viscoelastic-viscoplastic-viscodamage constitutive model for asphaltic materials. International Journal of Solids and Structures 48, 191–207.

Darabi, M.K., Abu Al-Rub, R.K., Masad, E.A., Little, D.N., 2011b. Thermodynamic based model for coupling temperature-dependent viscoelastic, viscoplastic, and viscodamage constitutive behavior of bituminous materials. International Journal for Numerical and Analytical Methods in Geomechanics. doi:10.1002/nag.1030.

Eggeler, G., Hornbogen, E., Yawny, A., Heckmann, A., Wagner, M., 2004. Structural and functional fatigue of niti shape memory alloys. Materials Science and Engineering a-Structural Materials Properties Microstructure and Processing 378, 24–33.

Fremond, M., Nedjar, B., 1996. Damage, gradient of damage and principle of virtual power. International Journal of Solids and Structures 33, 1083–1103.

Guo, Y.F., Guo, W.L., 2006. Self-healing properties of flaws in nanoscale materials: Effects of soft and hard molecular dynamics simulations and boundaries studied using a continuum mechanical model. Physical Review B 73, 1–7.

Hassan, T., Corona, E., Kyriakides, S., 1992. Ratcheting in cyclic plasticity. Part ii: multiaxial behavior. International Journal of Plasticity 8, 117–146.

Jacobsen, S., Marchand, J., Boisvert, L., 1996. Effect of cracking and healing on chloride transport in opc concrete. Cement and Concrete Research 26, 869–881.

Kachanov, L.M., 1958. On time to rupture in creep conditions (in russian). Izviestia Akademii Nauk SSSR, Otdelenie Tekhnicheskikh Nauk 8, 26–31.

Kachanov, L.M., 1986. Introduction to Continuum Damage Mechanics. M. Nijhoff, Dordrecht , Boston, MA.

Karsan, I.D., Jirsa, J.O., 1969. Behavior of concrete under compressive loadings. ASCE Journal of the Structural Division 95, 2543–2563.

Kessler, M.R., 2007. Self-healing: A new paradigm in materials design. Proceedings of the Institution of Mechanical Engineers Part G-Journal of Aerospace Engineering 221, 479–495.

Kessler, M.R., White, S.R., 2001. Self-activated healing of delamination damage in woven composites. Composites Part a-Applied Science and Manufacturing 32, 683–699.

Kim, Y.R., Little, D.N., 1990. One-dimensional constitutive modeling of asphalt concrete. Journal of Engineering Mechanics (ASCE) 116, 751–772.

Krajcinovic, D., 1996. Damage Mechanics. Elsevier, Amsterdam.

Lee, J., Fenves, G.L., 1998. A plastic-damage model for cyclic loading of concrete structures. Journal of Engineering Mechanics (ASCE) 124, 892–900.

Lee, H., Peng, K., Wang, J., 1985. An anisotropic damage criterion for deformation instability and its application to forming limit analysis of metal plates. Engineering Fracture Mechanics 21, 1031–1054.

Lemaître, J., Chaboche, J.-L., 1990. Mechanics of Solid Materials. Cambridge University Press, Cambridge.

Lemaître, J., Desmorat, R., Sauzay, M., 2000. Anisotropic damage law of evolution. European Journal of Mechanics a-Solids 19, 187–208.

Little, D.N., Bhasin, A., 2007. Exploring mechanisms of healing in asphalt mixtures and quantifying its impact. In: van der Zwaag, S. (Ed.), Self healing Materials. Springer, Dordrecht, The Netherlands, pp. 205–218.

Maugin, G.A., Muschik, W., 1994. Thermodynamics with internal variables. Part i: general concepts. Journal of Non-Equilibrium Thermodynamics 19, 217–249.

Miao, S., Wang, M.L., Schreyer, H.L., 1995. Constitutive models for healing of materials with application to compaction of crushed rock-salt. Journal of Engineering Mechanics (ASCE) 121, 1122–1129.

Mirmiran, A., Zagers, K., Yuan, W., 2000. Nonlinear finite element modeling of concrete confined by fiber composites. Finite Elements in Analysis and Design 35, 79–96.

Ortiz, M., 1985. A constitutive theory for the inelastic behavior of concrete. Mechanics of Materials 4, 67–93.

Palermo, D., Vecchio, F.J., 2004. Compression field modeling of reinforced concrete subjected to reversed loading: Verification. ACI Structural Journal 101, 155–164.

Perzyna, P., 1971. Thermodynamic theory of viscoplastcity. Advances in Applied Mechanics 11, 313–354.

Rabotnov, I.U.N., 1969a. Creep Problems in Structural Members. North-Holland Pub. Co., Amsterdam, London.

Rabotnov, I.U.N., 1969b. Creep Problems in Structural Members. North-Holland Pub. Co., Amsterdam, London.

Ramm, W., Biscoping, M., 1998. Autogenous healing and reinforcement corrosion of water-penetrated separation cracks in reinforced concrete. Nuclear Engineering and Design 179, 191–200.

Reinhardt, H.W., Jooss, M., 2003. Permeability and self-healing of cracked concrete as a function of temperature and crack width. Cement and Concrete Research 33, 981–985.

Rice, J.R., 1971. Inelastic constitutive relations for solids: An internal-variable theory and its application to metal plasticity. Journal of the Mechanics and Physics of Solids 19, 433–455.

Rodeo, S.A., Arnoczky, S.P., Torzilli, P.A., Hidaka, C., Warren, R.F., 1993. Tendon-healing in a bone tunnel: A biomechanical and histological study in the dog. Journal of Bone and Joint Surgery-American 75A, 1795–1803.

Rong, M.Z., Zhang, M.Q., Zhang, W., 2007. A novel self-healing epoxy system with microencapsulated epoxy and imidazole curing agent. Advanced Composites Letters 16, 167–172.

Schapery, R.A., 1969. Further development of a thermodynamic constitutive theory: Stress formulation. Purdue University, Purdue Resarch Foundation, Lafayette, IN.

Shizawa, K., Zbib, H.M., 1999. A thermodynamical theory of gradient elastoplasticity with dislocation density tensor I: Fundamentals. International Journal of Plasticity 15, 899–938.

Sima, J.F., Roca, P., Molins, C., 2008. Cyclic constitutive model for concrete. Engineering Structures 30, 695–706.

Simpson, A.H.R.W., Gardner, T.N., Evans, M., Kenwright, J., 2000. Stiffness, strength and healing assessment in different bone fractures – a simple mathematical model. Injury 31, 777–781.

Sinha, B.P., Gerstle, K.H., Tulin, L.G., 1964. Stress–strain relations for concrete under cyclic loading. ACI Journal Proceedings 61, 195–212.

Strauer, B.E., Brehm, M., Zeus, T., Kostering, M., Hernandez, A., Sorg, R.V., Kogler, G., Wernet, P., 2002. Repair of infarcted myocardium by autologous intracoronary mononuclear bone marrow cell transplantation in humans. Circulation 106, 1913–1918.

Voyiadjis, G.Z., Kattan, P.I., 1990. A coupled theory of damage mechanics and finite strain elasto-plasticity–ii. Damage and finite strain plasticity. International Journal of Engineering Science 28, 505–524.

Voyiadjis, G.Z., Kattan, P.I., 1993. Damage of fiber-reinforced composite-materials with micromechanical characterization. International Journal of Solids and Structures 30, 2757–2778.

Voyiadjis, G.Z., Kattan, P.I., 1999. Advances in Damage Mechanics: Metals and Metals Matrix Composites. Elsevier, Oxford.

Voyiadjis, G.Z., Thiagarajan, G., 1997. Micro and macro anisotropic cyclic damage-plasticity models for mmcs. International Journal of Engineering Science 35, 467–484.

Voyiadjis, G.Z., Abu Al-Rub, R.K., Palazotto, A.N., 2004. Thermodynamic framework for coupling of non-local viscoplasticity and non-local anisotropic viscodamage for dynamic localization problems using gradient theory. International Journal of Plasticity 20, 981–1038.

Voyiadjis, G.Z., Shojaei, A., Li, G., 2011. A thermodynamic consistent damage and healing model for self healing materials. International Journal of Plasticity 27, 1025–1044.

Werner, S., Grose, R., 2003. Regulation of wound healing by growth factors and cytokines. Physiological Reviews 83, 835–870.

White, S.R., Sottos, N.R., Geubelle, P.H., Moore, J.S., Kessler, M.R., Sriram, S.R., Brown, E.N., Viswanathan, S., 2001. Autonomic healing of polymer composites. Nature 409, 794–797.

White, S.R., Caruso, M.M., Moore, J.S., 2008. Autonomic healing of polymers. Mrs Bulletin 33, 766–769.

Wool, R.P., Oconnor, K.M., 1981. A theory of crack healing in polymers. Journal of Applied Physics 52, 5953–5963.

Yasko, A.W., Lane, J.M., Fellinger, E.J., Rosen, V., Wozney, J.M., Wang, E.A., 1992. The healing of segmental bone defects, induced by recombinant human bone morphogenetic protein (rhbmp-2): A radiographic, histological, and biomechanical study in rats. Journal of Bone and Joint Surgery-American 74A, 659–670.

Yin, T., Rong, M.Z., Zhang, M.Q., 2008. Self-healing of cracks in epoxy composites. Multi-Functional Materials and Structures, 282–285.

Yuan, Y.C., Yin, T., Rong, M.Z., Zhang, M.Q., 2008. Self healing in polymers and polymer composites. Concepts, realization and outlook: A review. Express Polymer Letters 2, 238–250.

Ziegler, H., 1977. An Introduction to Thermodynamics. North-Holland Pub. Co., Amsterdam.

Ziegler, H., 1983. An Introduction to Thermomechanics, 2nd ed. North-Holland Pub. Co., Amsterdam.

Ziegler, H., Wehrli, C., 1987. The derivation of constitutive relations from the free energy and the dissipation function. In: Theodore, Y.W., John, W.H. (Eds.), Advances in Applied Mechanics. Elsevier, Amsterdam, pp. 183–238.